

Supplementary information

Impact of Co^{2+} substitution by Fe^{2+} on the thermal behavior of a hydrated fluoride, precursor of a mixed iron-based oxyfluoride with reduced cobalt content as efficient OER electrocatalyst

Alexandre Terry,^{1,2} Guillaume Duval,¹ Samuel Mathiot,¹ Jean-Marc Grenèche,¹ Ralf Weisbarth,² Edouard Boivin,¹ Vincent Maisonneuve,¹ Annie Hémon-Ribaud,¹ Nikolay Kornienko,² Amandine Guiet,^{1,*} Jérôme Lhoste^{1,*}

¹Institut des Molécules et Matériaux du Mans, UMR 6283 CNRS, Le Mans Université, Avenue Olivier Messiaen, 72085 Le Mans Cedex 9, France

²Institute of Inorganic Chemistry, University of Bonn, Gerhard-Domagk-Str. 1, 53121 Bonn, Germany

* corresponding authors – jerome.lhoste@univ-lemans.fr and amandine.guiet@univ-lemans.fr

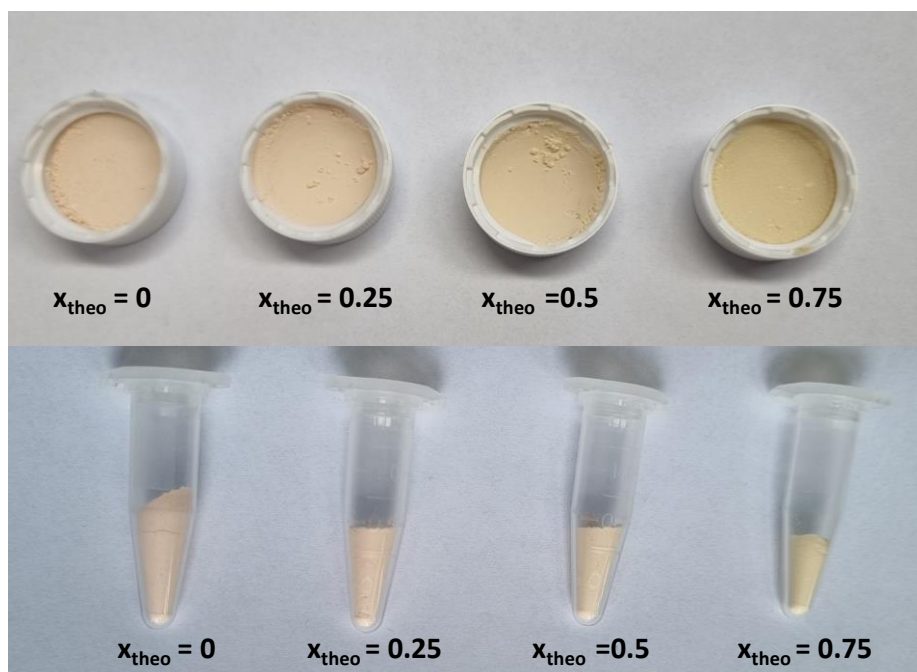


Figure S1: Photo of $(\text{Co}_{1-x}\text{Fe}_x)^{2+}\text{Fe}^{3+}\text{F}_5(\text{H}_2\text{O})_7$ polycrystalline powders, yellowing according to Fe^{2+} amount. This color evolution evidences the substitution of Co^{2+} by Fe^{2+} .

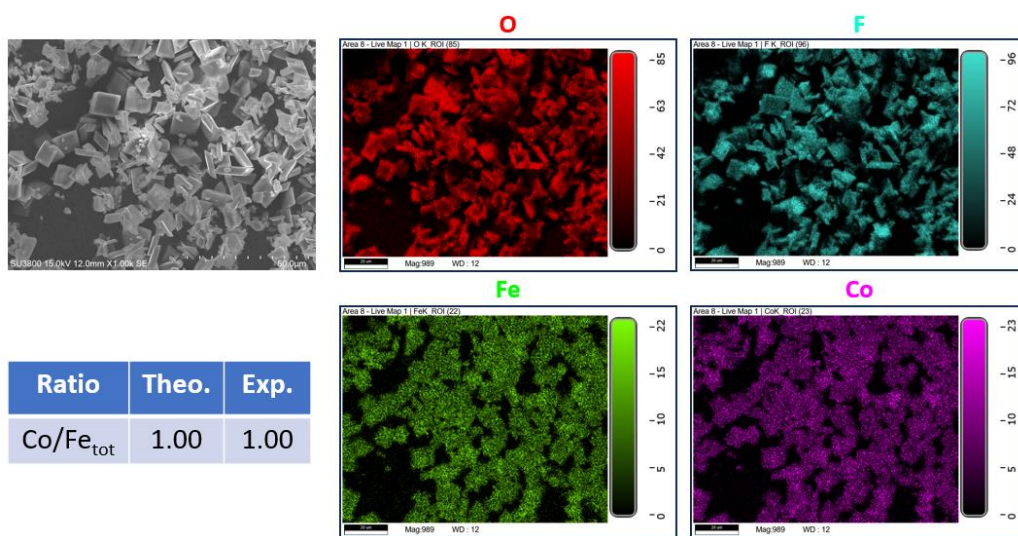


Figure S2: SEM images and elemental mapping of $\text{Co}^{2+}\text{Fe}^{3+}\text{F}_5(\text{H}_2\text{O})_7$.

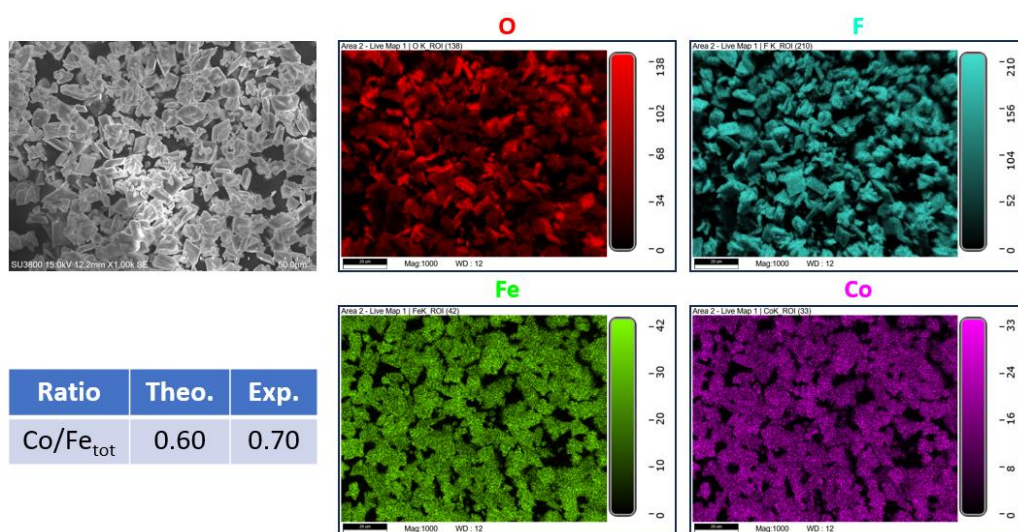


Figure S3: SEM images and elemental mapping of $(\text{Co}_{0.75}\text{Fe}_{0.25})^{2+}\text{Fe}^{3+}\text{F}_5(\text{H}_2\text{O})_7$.

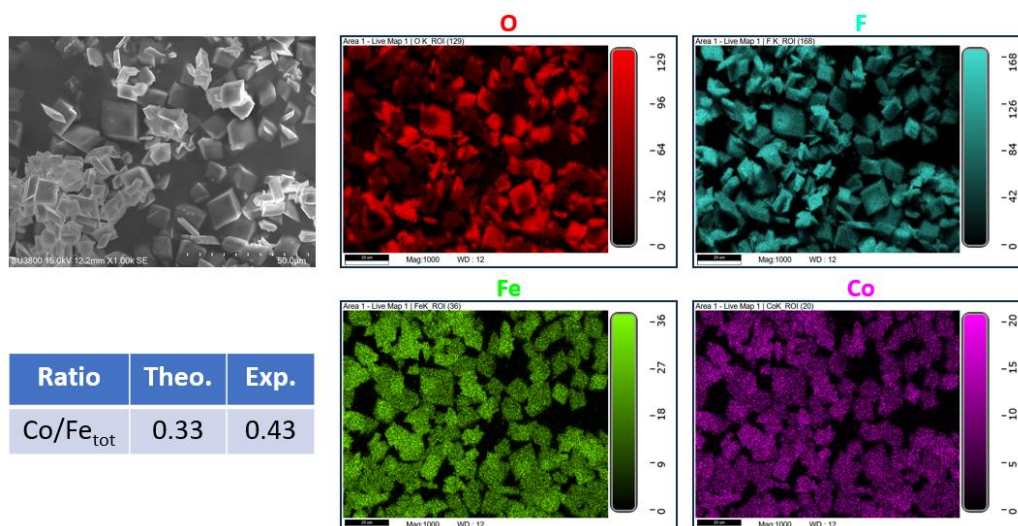


Figure S4: SEM images and elemental mapping of $(\text{Co}_{0.5}\text{Fe}_{0.5})^{2+}\text{Fe}^{3+}\text{F}_5(\text{H}_2\text{O})_7$.

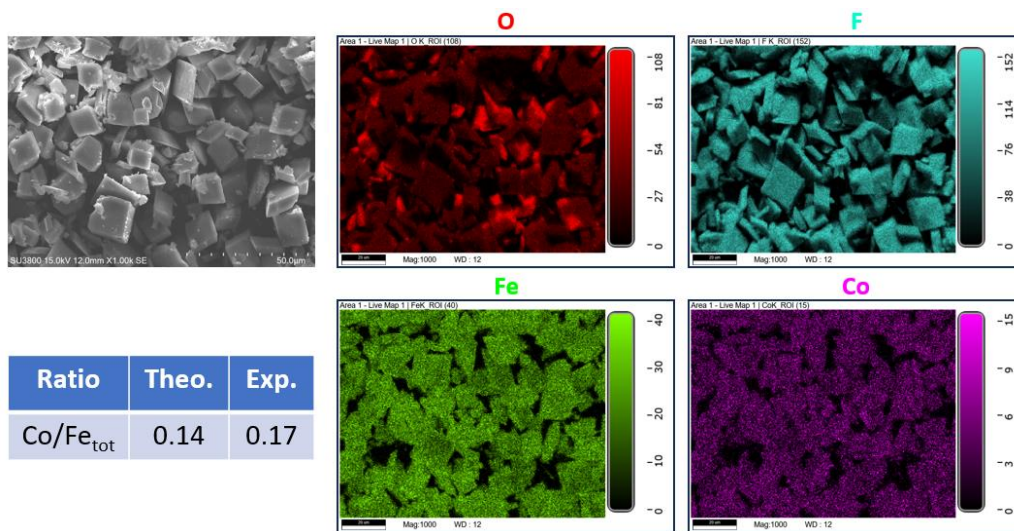
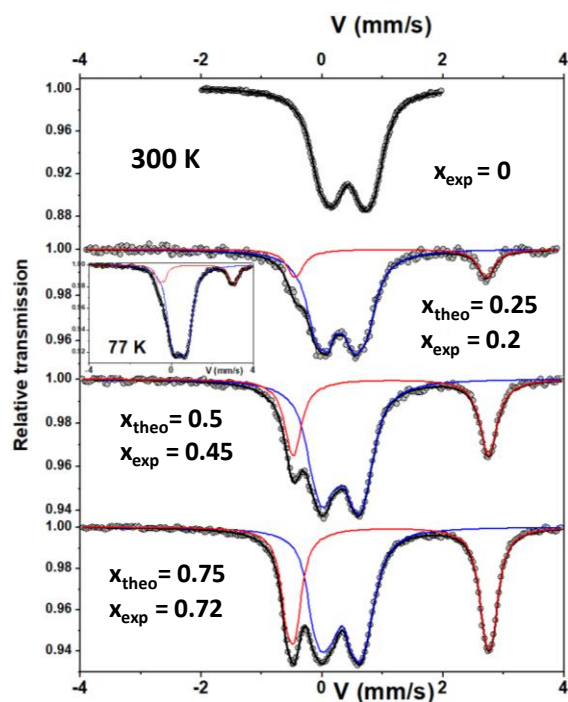


Figure S5: SEM images and elemental mapping of $(\text{Co}_{0.25}\text{Fe}_{0.75})^{2+}\text{Fe}^{3+}\text{F}_5(\text{H}_2\text{O})_7$.



	T (K)	Fe ⁿ⁺	IS (mm/s) ± 0.02	ΔE _Q (mm/s) ± 0.02	% ± 2
$x_{\text{exp}} = 0$	300	Fe ³⁺	<0.43>	<0.60>	100
$x_{\text{theo}} = 0.25$	300	Fe ³⁺	<0.43>	<0.60>	83
		Fe ²⁺	1.26	3.13	17
$x_{\text{exp}} = 0.2$	77	Fe ³⁺	<0.54>	<0.59>	83
		Fe ²⁺	<1.40>	<3.52>	17
$x_{\text{theo}} = 0.5$	300	Fe ³⁺	<0.44>	<0.59>	69
		Fe ²⁺	1.26	3.20	31
$x_{\text{theo}} = 0.75$	300	Fe ³⁺	<0.44>	<0.58>	58
		Fe ²⁺	<1.25>	<3.22>	42

Figure S6: ^{57}Fe Mössbauer spectra and refined values of the hyperfine parameters resulting from the ^{57}Fe Mössbauer spectra of $(\text{Co}_{1-x}\text{Fe}_x)^{2+}\text{Fe}^{3+}\text{F}_5(\text{H}_2\text{O})_7$ at 300 K and 77 K (only for $x_{\text{theo}} = 0.25$, inset).

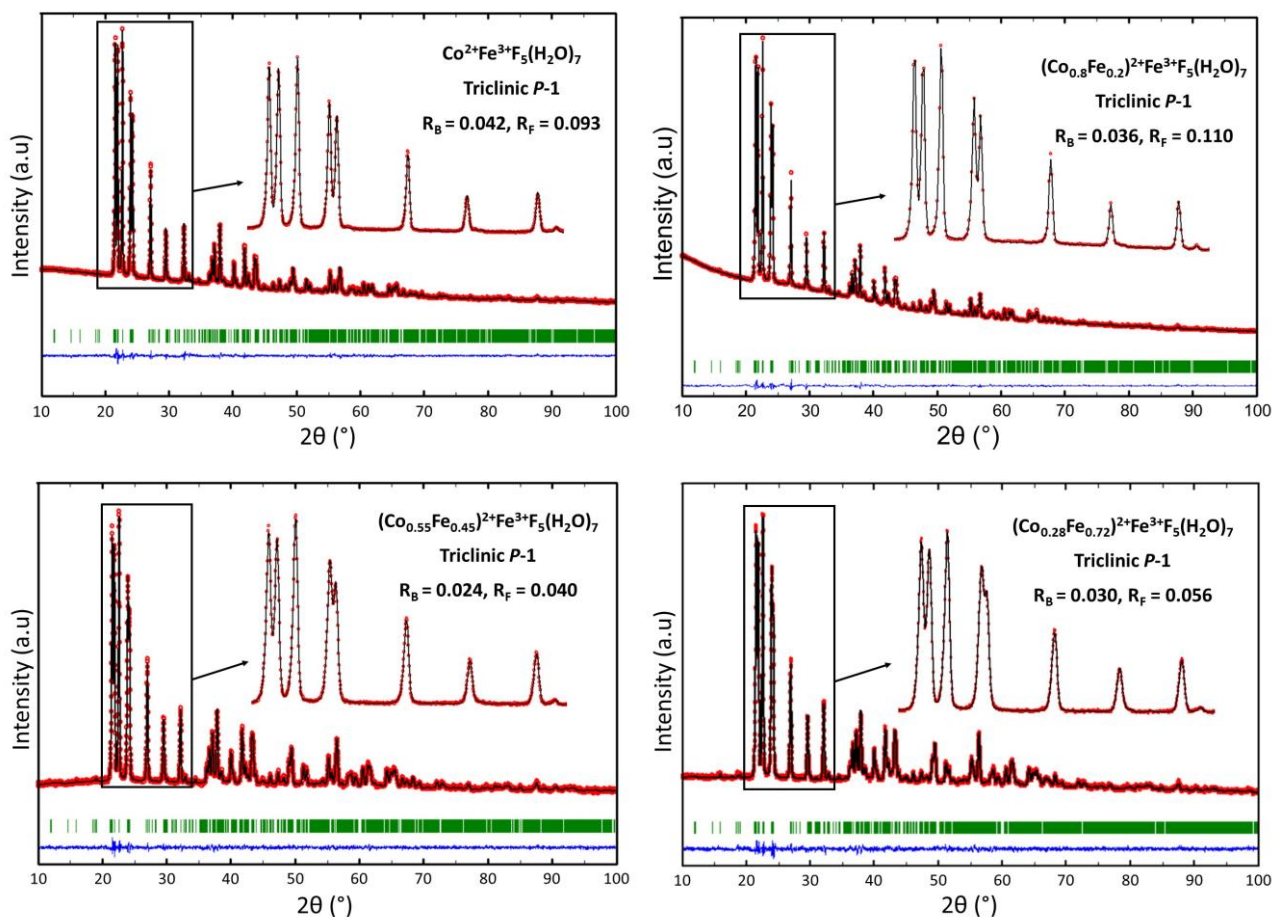


Figure S7: Rietveld refinements of the powder X-ray diffraction patterns of $(\text{Co}_{1-x}\text{Fe}_x)^{2+}\text{Fe}^{3+}\text{F}_5(\text{H}_2\text{O})_7$ (x_{exp}).

Table S1. Summary of crystallographic data of the $(\text{Co}_{1-x}\text{Fe}_x)^{2+}\text{Fe}^{3+}\text{F}_5(\text{H}_2\text{O})_7$ series (Triclinic, *P*-1) measured with $\text{Co K}\alpha$.

Solid solution	$(\text{Co}_{1-x}\text{Fe}_x)^{2+}\text{Fe}^{3+}\text{F}_5(\text{H}_2\text{O})_7$				
	x_{exp}	0	0.2	0.45	0.72
Molecular weight ($\text{g}\cdot\text{mol}^{-1}$)		335.88	335.26	334.49	333.65
<i>a</i> (Å)		6.525(1)	6.540(1)	6.560(1)	6.574(1)
<i>b</i> (Å)		8.841(1)	8.854(1)	8.863(1)	8.863(1)
<i>c</i> (Å)		8.979(1)	8.978(1)	8.977(1)	8.972(1)
α (°)		104.071(1)	103.933(1)	103.824(1)	103.658(1)
β (°)		97.080(1)	97.054(1)	96.988(1)	96.934(1)
γ (°)		95.377(1)	95.485(1)	95.496(1)	95.470(1)
<i>V</i> (Å ³), <i>Z</i>		494.51(2), 2	496.52(3), 2	498.81(3), 2	500.17(3), 2
ρ_{calc} ($\text{g}\cdot\text{cm}^{-3}$)		2.256	2.242	2.227	2.215
2θ range (°)		5 – 140	10 – 120	10 – 120	10 – 120
Unique reflections		2519	2008	2326	2355
Refined parameters		81	71	84	79
χ^2		2.42	2.56	0.93	1.05
R_p/R_{wp}		0.118/0.073	0.087/0.053	0.111/0.069	0.118/0.074
R_B/R_f		0.042/0.093	0.034/0.110	0.024/0.040	0.030/0.05695

Table S2. Atomic coordinates and equivalent isotropic displacement parameters of Co²⁺Fe³⁺F₅(H₂O)₇.

Atom	site	x	y	z	τ^a	B_{eq} (Å ²)
Fe(1)	1a	0	0	0	1	4.42(7) ^b
Fe(2)	1g	0	½	½	1	4.42(7) ^b
Co(1)	1e	½	½	0	1	4.42(7) ^b
Co(2)	1f	½	0	½	1	4.42(7) ^b
F(1)/O(1)	2i	0.1263(14)	0.9363(9)	0.8019(11)	0.5/0.5	5.38(9) ^c
F(3)	2i	0.9193(15)	0.1793(11)	0.9407(10)	1	5.38(9) ^c
F(4)	2i	0.7283(20)	0.8819(14)	0.8985(12)	1	5.38(9) ^c
F(2)/O(2)	2i	0.9584(18)	0.7336(15)	0.5426(11)	0.5/0.5	5.38(9) ^c
F(5)	2i	0.7196(18)	0.4314(13)	0.4196(11)	1	5.38(9) ^c
F(6)	2i	0.0547(16)	0.5043(12)	0.3016(11)	1	5.38(9) ^c
O(3)	2i	0.8117(19)	0.5717(13)	0.0795(13)	1	5.38(9) ^c
O(4)	2i	0.4489(20)	0.7203(17)	0.0036(12)	1	5.38(9) ^c
O(5)	2i	0.5451(16)	0.4645(10)	0.7752(11)	1	5.38(9) ^c
O(6)	2i	0.2276(19)	-0.1184(14)	0.3798(13)	1	5.38(9) ^c
O(7)	2i	0.3389(15)	0.1223(11)	0.6541(11)	1	5.38(9) ^c
O(8)	2i	0.4723(17)	0.1667(12)	0.3815(10)	1	5.38(9) ^c

a) Constrained to fix values b) constrained to be equal c) constrained to be equal

Table S3. Selected inter-atomic distances (Å) of Co²⁺Fe³⁺F₅(H₂O)₇.

Fe(1)-F(1)/O(1) x2	2.030(10)	<Fe-F/O> = 2.044
Fe(1)-F(3) x2	1.890(10)	
Fe(1)-F(4) x2	1.964(12)	
Fe(2)-F(2)/O(2) x2	2.057(13)	<Fe-F> = 1.898
Fe(2)-F(5) x2	1.868(12)	
Fe(2)-F(6) x2	1.868(10)	
Co(1)-O(3) x2	2.056(12)	<Co-O> = 2.022
Co(1)-O(4) x2	2.000(15)	
Co(1)-O(5) x2	2.029(10)	
Co(2)-O(6) x2	2.012(11)	
Co(2)-O(7) x2	2.008(10)	
Co(2)-O(8) x2	2.025(11)	

Table S4. Atomic coordinates and equivalent isotropic displacement parameters of $(\text{Co}_{0.8}\text{Fe}_{0.2})^{2+}\text{Fe}^{3+}\text{F}_5(\text{H}_2\text{O})_7$

Atom	site	x	y	z	τ^a	B_{eq} (\AA^2)
Fe(1)	1a	0	0	0	1	5.48(11) ^b
Fe(2)	1g	0	½	½	1	5.48(11) ^b
Co(1)/Fe(3)	1e	½	½	0	0.8/0.2	5.48(11) ^b
Co(2)/Fe(4)	1f	½	0	½	0.8/0.2	5.48(11) ^b
F(1)/O(1)	2i	0.1028(22)	0.9287(16)	0.7956(18)	0.5/0.5	7.31(13) ^c
F(3)	2i	0.9261(24)	0.1794(16)	0.9372(14)	1	7.31(13) ^c
F(4)	2i	0.7275(32)	0.8920(22)	0.9049(17)	1	7.31(13) ^c
F(2)/O(2)	2i	0.9541(35)	0.7209(28)	0.5323(22)	0.5/0.5	7.31(13) ^c
F(5)	2i	0.7285(28)	0.4415(19)	0.4167(17)	1	7.31(13) ^c
F(6)	2i	0.0578(25)	0.5077(19)	0.3072(16)	1	7.31(13) ^c
O(3)	2i	0.8079(27)	0.5756(21)	0.0757(19)	1	7.31(13) ^c
O(4)	2i	0.4527(34)	0.7296(27)	0.0192(23)	1	7.31(13) ^c
O(5)	2i	0.5459(25)	0.4638(17)	0.7724(17)	1	7.31(13) ^c
O(6)	2i	0.2287(28)	-0.1302(20)	0.3729(18)	1	7.31(13) ^c
O(7)	2i	0.3312(23)	0.1191(16)	0.6470(16)	1	7.31(13) ^c
O(8)	2i	0.4774(29)	0.1652(18)	0.3803(15)	1	7.31(13) ^c

a) Constrained to fix values b) constrained to be equal c) constrained to be equal

Table S5. Selected inter-atomic distances (\AA) of $(\text{Co}_{0.8}\text{Fe}_{0.2})^{2+}\text{Fe}^{3+}\text{F}_5(\text{H}_2\text{O})_7$.

Fe(1)-F(1)/O(1) x2	2.012(15)	<Fe-F/O> = 1.991
Fe(1)-F(3) x2	1.894(15)	
Fe(1)-F(4) x2	1.933(17)	
Fe(2)-F(2)/O(2) x2	1.970(30)	<Fe-F> = 1.868
Fe(2)-F(5) x2	1.812(18)	
Fe(2)-F(6) x2	1.832(14)	
Co(1)/Fe(3)-O(3) x2	2.038(18)	<Co/Fe-O> = 2.039
Co(1)/Fe(3)-O(4) x2	2.060(30)	
Co(1)/Fe(3)-O(5) x2	2.055(15)	
Co(2)/Fe(4)-O(6) x2	2.062(16)	
Co(2)/Fe(4)-O(7) x2	1.997(13)	
Co(2)/Fe(4)-O(8) x2	2.019(16)	

Table S6. Atomic coordinates and equivalent isotropic displacement parameters of $(\text{Co}_{0.55}\text{Fe}_{0.45})^{2+}\text{Fe}^{3+}\text{F}_5(\text{H}_2\text{O})_7$.

Atom	site	x	y	z	τ^a	B_{eq} (\AA^2)
Fe(1)	1a	0	0	0	1	2.34(7) ^b
Fe(2)	1g	0	½	½	1	2.34(7) ^b
Co(1)/Fe(3)	1e	½	½	0	0.55/0.45	2.34(7) ^b
Co(2)/Fe(4)	1f	½	0	½	0.55/0.45	2.34(7) ^b
F(1)/O(1)	2i	0.1065(14)	0.9290(10)	0.7950(11)	0.5/0.5	3.63(8) ^c
F(3)	2i	0.9234(14)	0.1857(10)	0.9348(9)	1	3.63(8) ^c
F(4)	2i	0.7301(19)	0.8961(12)	0.9091(11)	1	3.63(8) ^c
F(2)/O(2)	2i	0.9561(19)	0.7265(15)	0.5331(14)	0.5/0.5	3.63(8) ^c
F(5)	2i	0.7106(19)	0.4359(12)	0.4138(12)	1	3.63(8) ^c
F(6)	2i	0.0626(15)	0.5044(11)	0.2987(12)	1	3.63(8) ^c
O(3)	2i	0.8173(17)	0.5761(12)	0.0835(13)	1	3.63(8) ^c
O(4)	2i	0.4494(20)	0.7316(15)	0.0151(14)	1	3.63(8) ^c
O(5)	2i	0.5506(17)	0.4599(12)	0.7688(11)	1	3.63(8) ^c
O(6)	2i	0.2181(16)	-0.1335(12)	0.3734(11)	1	3.63(8) ^c
O(7)	2i	0.3241(13)	0.1341(10)	0.6536(10)	1	3.63(8) ^c
O(8)	2i	0.4812(18)	0.1631(12)	0.3720(10)	1	3.63(8) ^c

a) Constrained to fix values b) constrained to be equal c) constrained to be equal

Table S7. Selected inter-atomic distances (\AA) of $(\text{Co}_{0.55}\text{Fe}_{0.45})^{2+}\text{Fe}^{3+}\text{F}_5(\text{H}_2\text{O})_7$

Fe(1)-F(1)/O(1) x2	2.028(9)	<Fe-F/O> = 2.020
Fe(1)-F(3) x2	1.962(9)	
Fe(1)-F(4) x2	1.904(10)	
Fe(2)-F(2)/O(2) x2	2.012(13)	<Fe-F> = 1.928
Fe(2)-F(5) x2	1.937(11)	
Fe(2)-F(6) x2	1.908(10)	
Co(1)/Fe(3)-O(3) x2	2.112(10)	<Co/Fe-O> = 2.100
Co(1)/Fe(3)-O(4) x2	2.086(13)	
Co(1)/Fe(3)-O(5) x2	2.093(10)	
Co(2)/Fe(4)-O(6) x2	2.130(9)	
Co(2)/Fe(4)-O(7) x2	2.124(8)	
Co(2)/Fe(4)-O(8) x2	2.053(10)	

Table S8. Atomic coordinates and equivalent isotropic displacement parameters of $(\text{Co}_{0.28}\text{Fe}_{0.72})^{2+}\text{Fe}^{3+}\text{F}_5(\text{H}_2\text{O})_7$

Atom	site	x	y	z	τ^a	B_{eq} (\AA^2)
Fe(1)	1a	0	0	0	1	2.75(7) ^b
Fe(2)	1g	0	½	½	1	2.75(7) ^b
Co(1)/Fe(3)	1e	½	½	0	0.28/0.72	2.75(7) ^b
Co(2)/Fe(4)	1f	½	0	½	0.28/0.72	2.75(7) ^b
F(1)/O(1)	2i	0.1040(14)	0.9212(12)	0.7916(12)	0.5/0.5	4.55(9) ^c
F(3)	2i	0.9283(15)	0.1912(12)	0.9369(9)	1	4.55(9) ^c
F(4)	2i	0.7277(19)	0.8936(13)	0.9104(12)	1	4.55(9) ^c
F(2)/O(2)	2i	0.9648(17)	0.7251(12)	0.5314(14)	0.5/0.5	4.55(9) ^c
F(5)	2i	0.7114(17)	0.4184(13)	0.4081(13)	1	4.55(9) ^c
F(6)	2i	0.0421(15)	0.4617(11)	0.2839(11)	1	4.55(9) ^c
O(3)	2i	0.8254(16)	0.5563(14)	0.0759(13)	1	4.55(9) ^c
O(4)	2i	0.4442(18)	0.7368(12)	0.0117(14)	1	4.55(9) ^c
O(5)	2i	0.5697(17)	0.5027(13)	0.7794(13)	1	4.55(9) ^c
O(6)	2i	0.2275(17)	-0.1333(12)	0.3717(12)	1	4.55(9) ^c
O(7)	2i	0.3208(14)	0.1376(11)	0.6481(11)	1	4.55(9) ^c
O(8)	2i	0.4837(21)	0.1544(13)	0.3664(11)	1	4.55(9) ^c

a) Constrained to fix values b) constrained to be equal c) constrained to be equal

Table S9. Selected inter-atomic distances (\AA) of $(\text{Co}_{0.28}\text{Fe}_{0.72})^{2+}\text{Fe}^{3+}\text{F}_5(\text{H}_2\text{O})_7$

Fe(1)-F(1)/O(1) x2	2.058(10)	<Fe-F/O> = 2.023
Fe(1)-F(3) x2	1.989(10)	
Fe(1)-F(4) x2	1.927(11)	
Fe(2)-F(2)/O(2) x2	1.988(10)	<Fe-F> = 1.958
Fe(2)-F(5) x2	1.970(10)	
Fe(2)-F(6) x2	1.946(10)	
Co(1)/Fe(3)-O(3) x2	2.139(9)	<Co/Fe-O> = 2.103
Co(1)/Fe(3)-O(4) x2	2.145(10)	
Co(1)/Fe(3)-O(5) x2	2.090(11)	
Co(2)/Fe(4)-O(6) x2	2.094(9)	
Co(2)/Fe(4)-O(7) x2	2.128(9)	
Co(2)/Fe(4)-O(8) x2	2.023(11)	

Crystallographic data (excluding structure factors) for the structures have been deposited with the Cambridge Crystallographic Data Centre as supplementary publication nos. CSD 2379403 ($(\text{Co}_{0.8}\text{Fe}_{0.2}^{2+}\text{Fe}^{3+}\text{F}_5(\text{H}_2\text{O})_7$ (**1**)), 2379404 ($(\text{Co}_{0.55}\text{Fe}_{0.45})^{2+}\text{Fe}^{3+}\text{F}_5(\text{H}_2\text{O})_7$ (**2**)), 2379405 ($(\text{Co}_{0.28}\text{Fe}_{0.72})^{2+}\text{Fe}^{3+}\text{F}_5(\text{H}_2\text{O})_7$ (**3**)). Copies of the data can be obtained, free of charge, on application to CCDC, 12 Union Road, Cambridge CB2 1EZ, UK, (fax: +44 1223 336033 or e-mail: deposit@ccdc.cam.ac.uk).

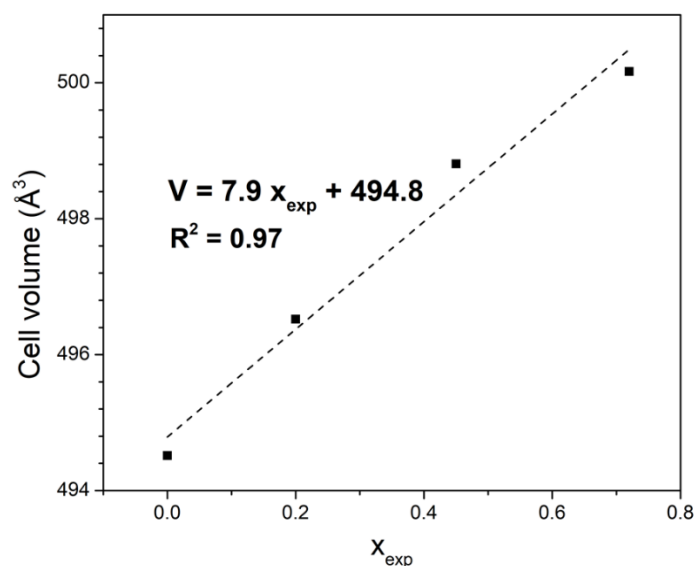


Figure S8: Variation of the unit cell volume of the $(\text{Co}_{1-x}\text{Fe}_x)^{2+}\text{Fe}^{3+}\text{F}_5(\text{H}_2\text{O})_7$ series with increasing Fe^{2+} substitution rate (x_{exp}).

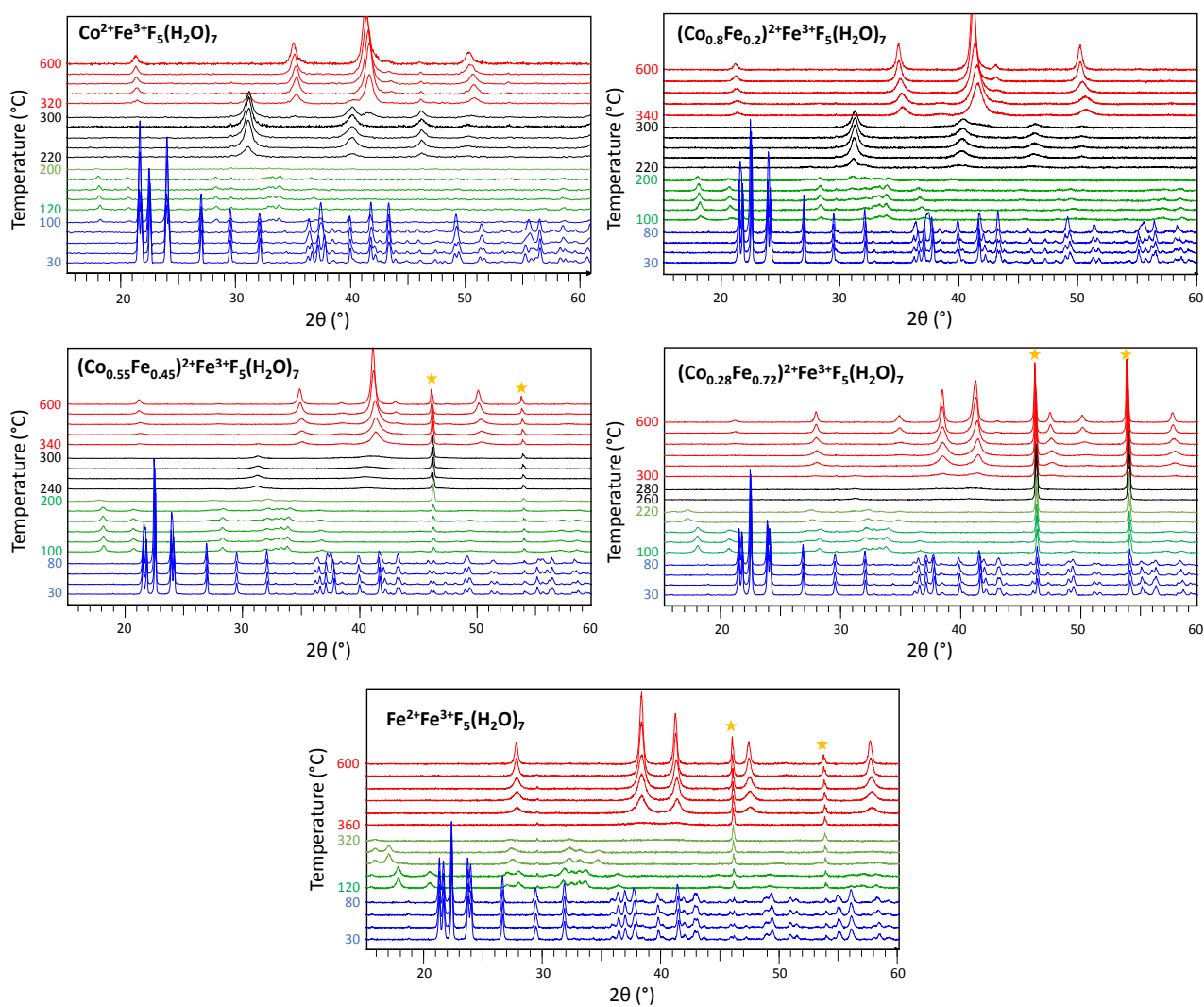


Figure S9: Thermal evolution of the X-ray diffractograms for $(\text{Co}_{1-x}\text{Fe}_x)^{2+}\text{Fe}^{3+}\text{F}_5(\text{H}_2\text{O})_7$ under ambient air. Diffraction peaks indicated with the yellow stars are peaks belonging to the sample holder, made with Pt.

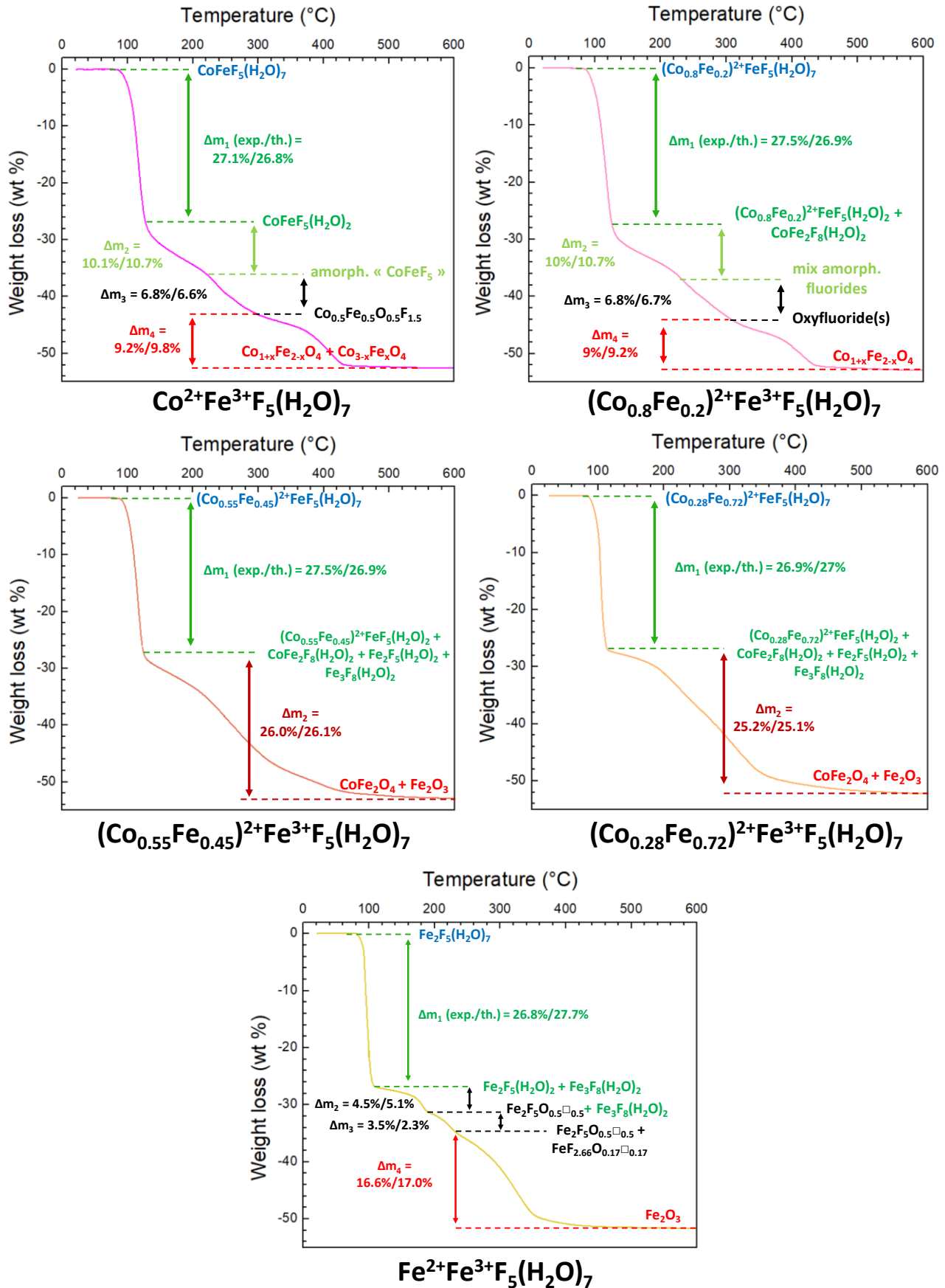


Figure S10: TGA analyses of $(\text{Co}_{1-x}\text{Fe}_x)^{2+}\text{Fe}^{3+}\text{F}_5(\text{H}_2\text{O})_7$ performed under ambient air.

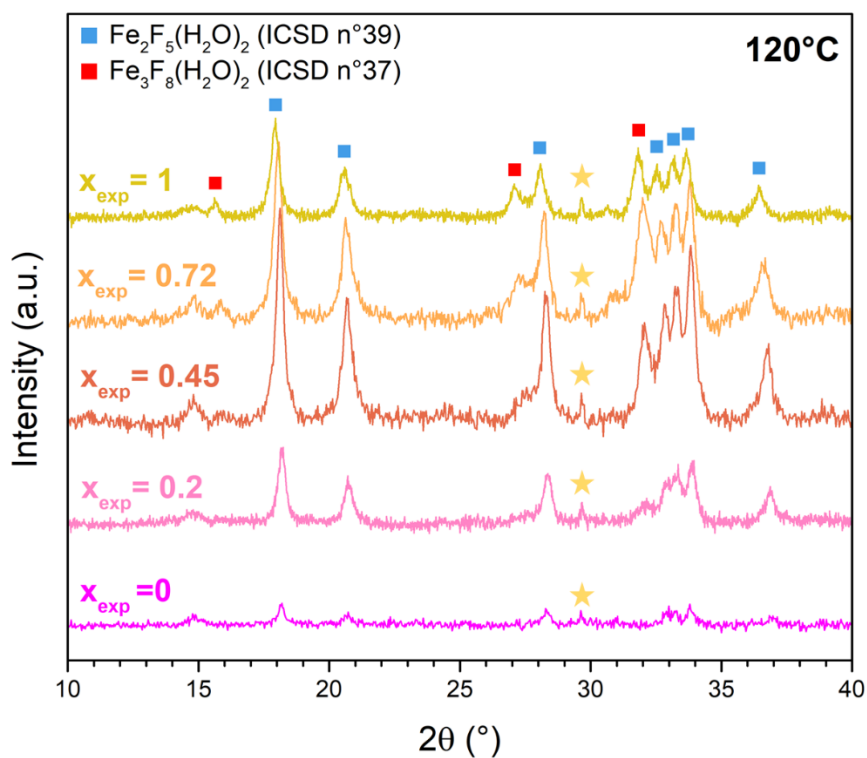


Figure S11: Powder X-ray diffraction patterns of the different $(\text{Co}_{1-x}\text{Fe}_x)^{2+}\text{Fe}^{3+}\text{F}_5(\text{H}_2\text{O})_7$ treated at 120°C . Peaks indicated by a yellow star belong to Pt sample holder.

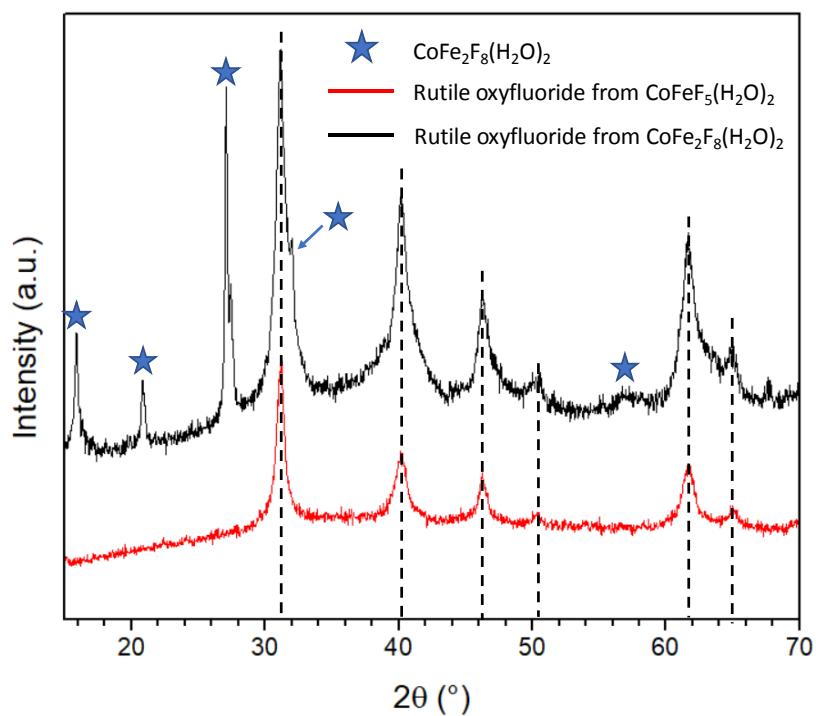


Figure S12: Powder X-ray diffraction patterns extracted from HT-XRD of $\text{CoFe}_5(\text{H}_2\text{O})_7$ and $\text{CoFe}_2\text{F}_8(\text{H}_2\text{O})_2$ treated respectively at 260°C and 300°C .

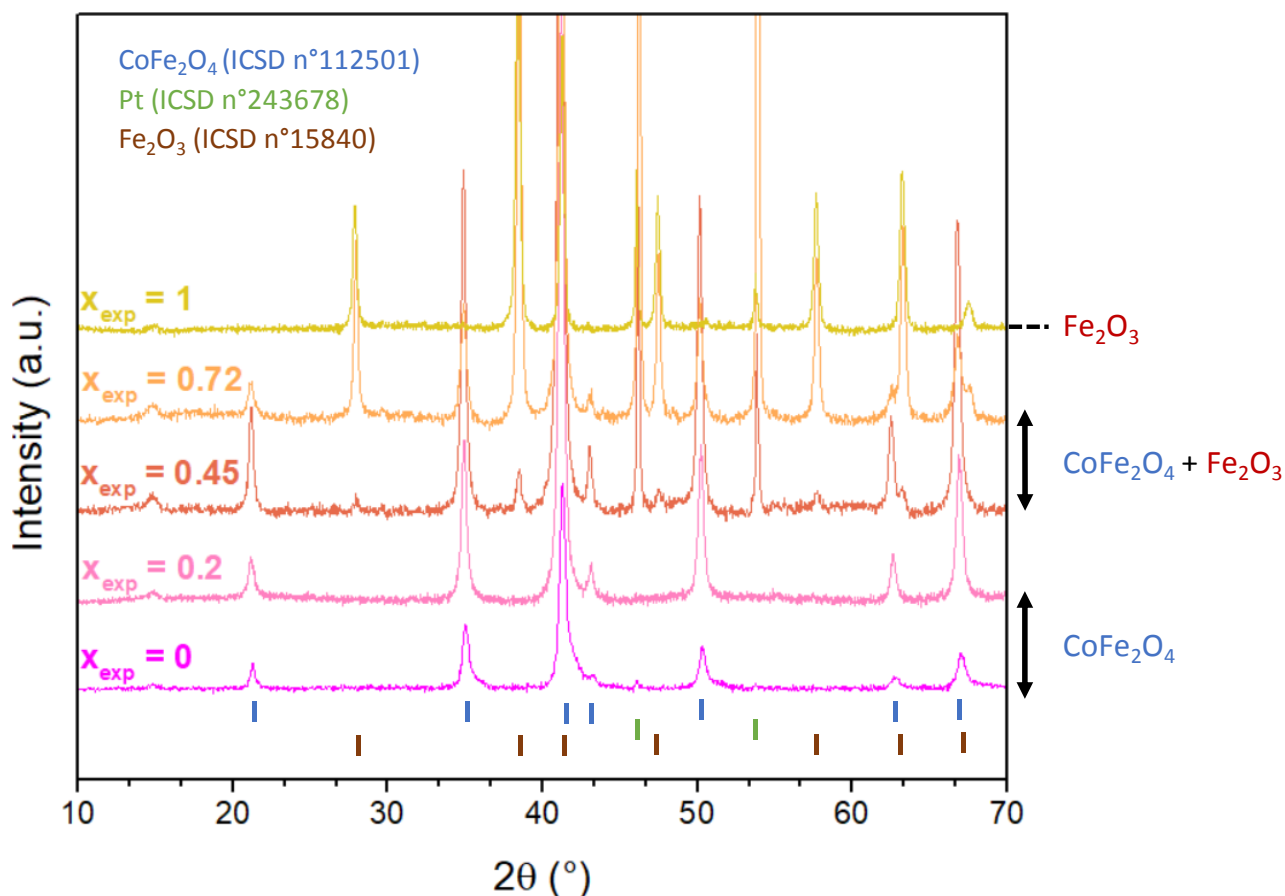


Figure S13: Powder X-ray diffraction patterns of the different $(\text{Co}_{1-x}\text{Fe}_x)^{2+}\text{Fe}^{3+}\text{F}_5(\text{H}_2\text{O})_7$ treated at 600°C . Peaks of Pt phase come from the sample carrier.

Rietveld refinements of the PXRD patterns at 120°C

For the Rietveld refinement of the different PXRD patterns at 120°C , we considered two different hypotheses. The first hypothesis supposes that the thermal degradation of $(\text{Co}_{1-x}\text{Fe}_x)^{2+}\text{Fe}^{3+}\text{F}_5(\text{H}_2\text{O})_7$ leads to a mix of $\text{MFeF}_5(\text{H}_2\text{O})_2$ and $\text{MFe}_2\text{F}_8(\text{H}_2\text{O})_2$ without substitution (e.g. $\text{M} = \text{Co}^{2+}$ or Fe^{2+}). The second hypothesis take in consideration a potential substitution in $\text{MFeF}_5(\text{H}_2\text{O})_2$ and/or $\text{MFe}_2\text{F}_8(\text{H}_2\text{O})_2$ ($\text{M} = \text{Co}^{2+}/\text{Fe}^{2+}$). The phases took in consideration for Rietveld refinement according to each hypothesis are summarized in the table below.

Table S10: Phases took in consideration for Rietveld refinements of PXRD patterns at 120°C according to the different hypothesis.

Hypothesis n°1	Hypothesis n°2
$\text{CoFeF}_5(\text{H}_2\text{O})_2$	$(\text{Co}_{1-x}\text{Fe}_x)^{2+}\text{Fe}^{3+}\text{F}_5(\text{H}_2\text{O})_2$
$\text{CoFe}_2\text{F}_8(\text{H}_2\text{O})_2$	$(\text{Co}_{1-x}\text{Fe}_x)^{2+}\text{Fe}^{3+}_2\text{F}_8(\text{H}_2\text{O})_2$
$\text{Fe}_2\text{F}_5(\text{H}_2\text{O})_2$	$\text{Fe}_2\text{F}_5(\text{H}_2\text{O})_2$
$\text{Fe}_3\text{F}_8(\text{H}_2\text{O})_2$	$\text{Fe}_3\text{F}_8(\text{H}_2\text{O})_2$

For the hypothesis n°2, $\text{Fe}_2\text{F}_5(\text{H}_2\text{O})_2$ and $\text{Fe}_3\text{F}_8(\text{H}_2\text{O})_2$ are only selected if Fe_2O_3 is observed at 600°C (i.e. $x_{\text{exp}} \geq 0.45$, see **Figure S17**) since according to HT-XRD of $\text{Fe}_2\text{F}_5(\text{H}_2\text{O})_7$, $\text{Fe}_2\text{F}_5(\text{H}_2\text{O})_2$ and $\text{Fe}_3\text{F}_8(\text{H}_2\text{O})_2$ leads both to Fe_2O_3 after thermal decomposition while for $\text{CoFeF}_5(\text{H}_2\text{O})_7$, no trace of Fe_2O_3 is observed, only spinel-type $\text{MM}'_2\text{O}_4$.

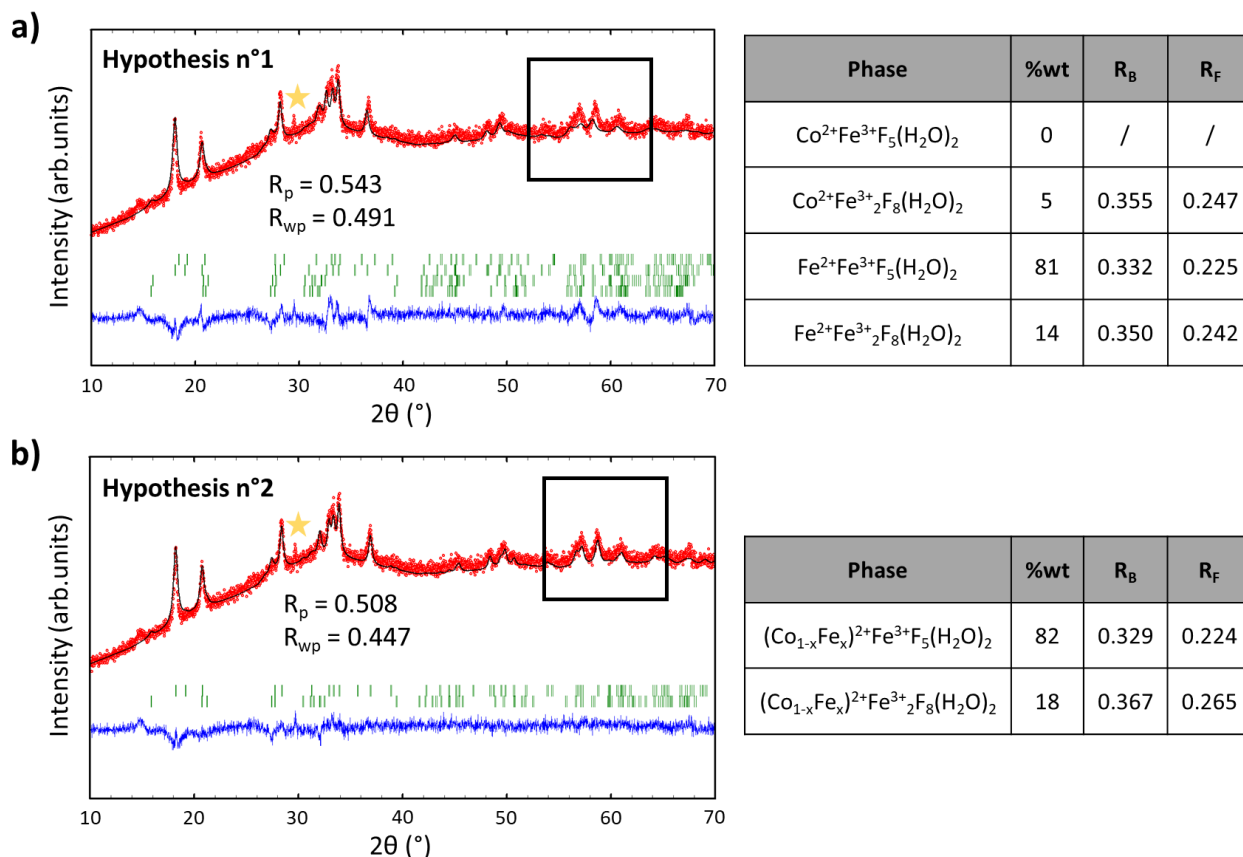
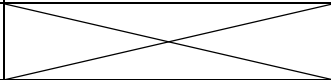
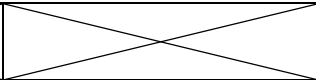


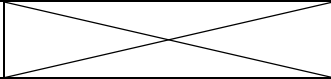
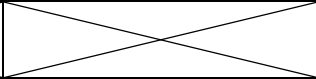


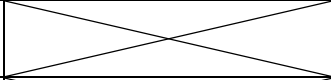
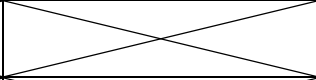
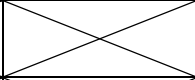
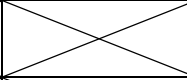
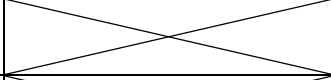
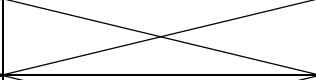
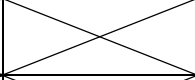
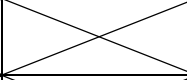
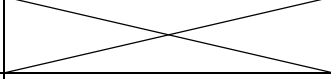
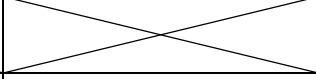
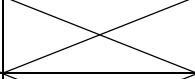
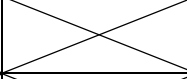


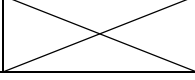
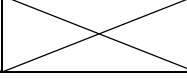


Figure S14: Rietveld refinements of the PXRD pattern of $(\text{Co}_{0.8}\text{Fe}_{0.2})^{2+}\text{FeF}_5(\text{H}_2\text{O})_7$ from the HT-XRD at 120°C according to hypothesis n°1 and hypothesis n°2, with mass proportion and structure factors for each phase given in the respective tables.

From these results, the hypothesis n°2 seems to be suitable to describe the system. In fact, the profile factors (R_p and R_{wp}) are better and the peaks fit better, as exemplified with the peaks between 56 and 60° . Also, the weight percentage is more in adequation with the initial composition because for hypothesis n°1, pure Fe^{2+} -phases are in majority compared to Co^{2+} -phases while $(\text{Co}_{0.8}\text{Fe}_{0.2})^{2+}\text{Fe}^{3+}\text{F}_5(\text{H}_2\text{O})_7$ contains four times more Co^{2+} than Fe^{2+} . In this way, hypothesis n°2 will be used for all the others compositions. All the phases took in consideration for Rietveld refinements of the different compositions $(\text{Co}_{1-x}\text{Fe}_x)^{2+}\text{Fe}^{3+}\text{F}_5(\text{H}_2\text{O})_7$ are summarized in **Table S11** below. Two additional compositions, $x = 0.33$ and 0.66 were added in this study to collect more data, even though not mentioned in the main article.

Table S11. Selected phases for Rietveld refinement of PXRD patterns at 120°C.

Compound	Phases taking in consideration for Rietveld Refinement			
x_{exp}	$(Co_{1-x}Fe_x)^{2+}Fe^{3+}F_5(H_2O)_2^*$	$(Co_{1-x}Fe_x)^{2+}Fe_2F_8(H_2O)_2^*$	$Fe_2F_5(H_2O)_2^{**}$	$Fe_3F_8(H_2O)_2^{**}$
0	Sample not refine because too amorphous.			
0.2				
"0.33"				
0.45				
"0.66"				
0.72				
1				

* Unit cell parameters refined ; **Unit cell parameters fixed

The atomic positions were not refined. Only the unit cell parameters.

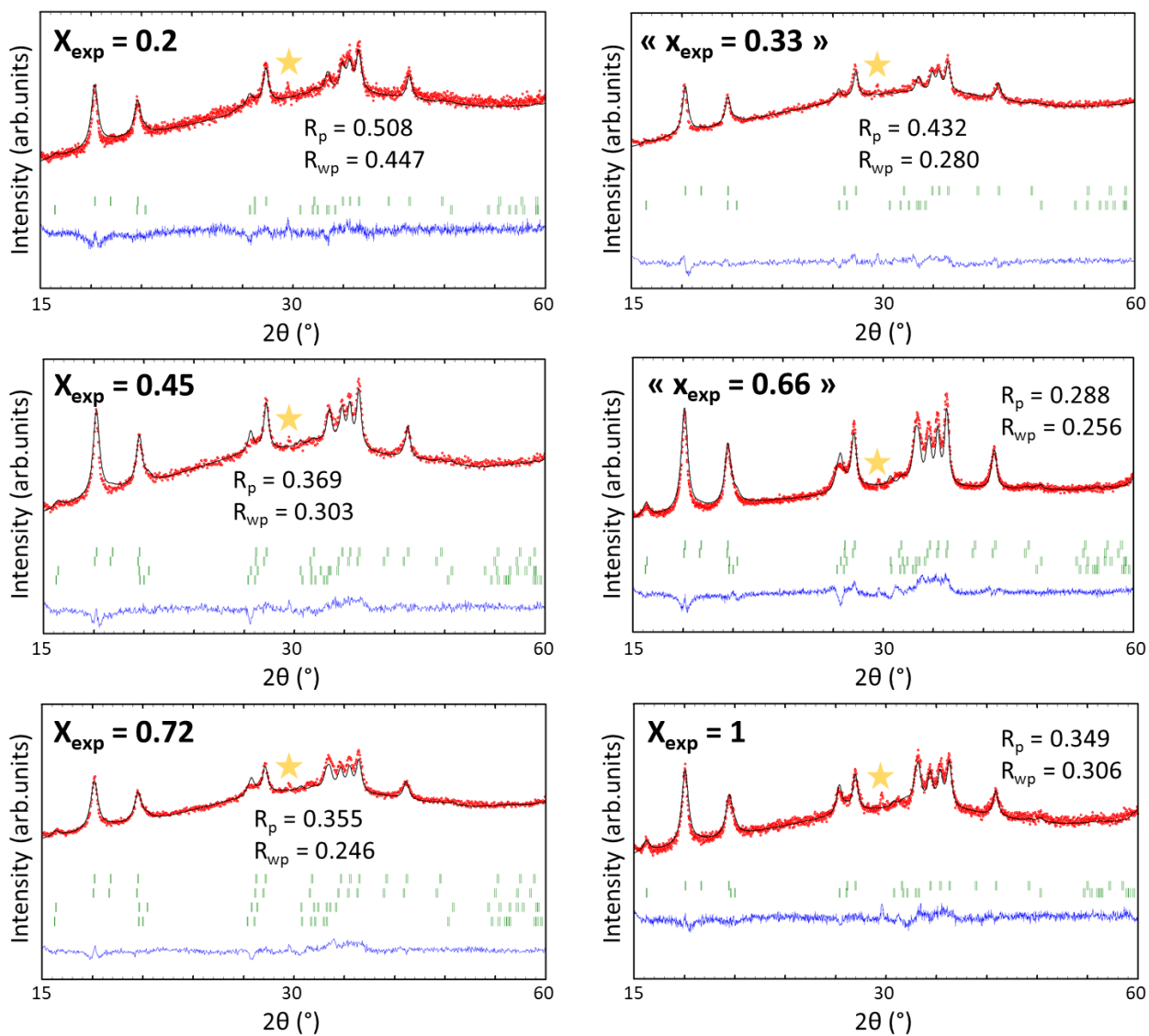


Figure S15: Rietveld Refinements of the PXRD patterns at 120°C of $(\text{Co}_{1-x}\text{Fe}_x)^{2+}\text{Fe}^{3+}\text{F}_5(\text{H}_2\text{O})_7$.

Table S12. Results of the Rietveld refinements of PXRD patterns at 120°C.

Compound	Phases taking in consideration for Rietveld Refinement							
	$(\text{Co}_{1-x}\text{Fe}_x)^{2+}\text{FeF}_5(\text{H}_2\text{O})_2$		$\text{CoFe}_2\text{F}_8(\text{H}_2\text{O})_2$		$\text{Fe}_2\text{F}_5(\text{H}_2\text{O})_2^{**}$		$\text{Fe}_3\text{F}_8(\text{H}_2\text{O})_2^{**}$	
x_{exp}	%W	%X	%W	%X	%W	%X	%W	%X
0.2	82	87	18	13	/	/	/	/
"0.33"	78	84	22	16	/	/	/	/
0.45	69	74	21	15	10	11	≈ 0	≈ 0
"0.66"	42	46	21	16	26	29	11	9
0.72	58	64	25	18	12	14	5	4
1	/	/	/	/	68	75	32	25

According to the quality of XRD data (broad and asymmetric peaks, low counting time), these percentages are just an approximation, as illustrated with the result for $x = 0.72$ which is out of the trend.

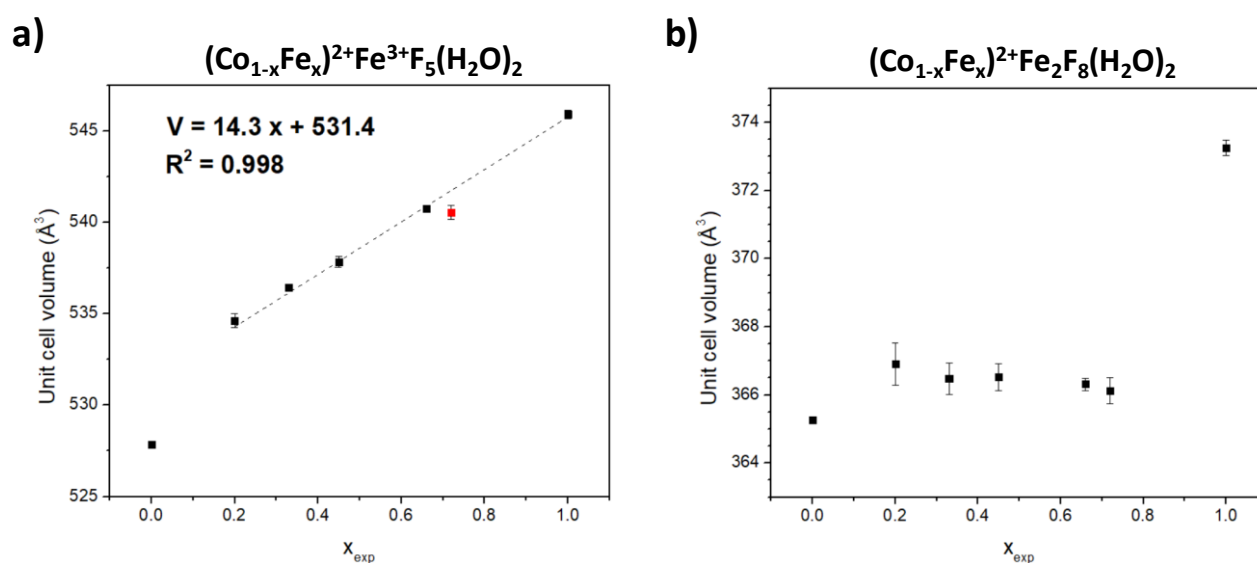


Figure S16: Evolution of the unit cell volume of $(\text{Co}_{1-x}\text{Fe}_x)^{2+}\text{Fe}^{3+}\text{F}_5(\text{H}_2\text{O})_2$ (a) and $(\text{Co}_{1-x}\text{Fe}_x)^{2+}\text{Fe}_2\text{F}_8(\text{H}_2\text{O})_2$ (b) as a function of x_{exp} , extracted from Rietveld refinements of PXRD patterns at 120°C.

The volume of $\text{Co}^{2+}\text{Fe}^{3+}\text{F}_5(\text{H}_2\text{O})_2$ was extracted from the ICSD database (ICSD n°113428). Such gap of this point, comparing to the others respecting perfectly the Vegard's Law (linear evolution of the unit cell volume in a solid solution), could be explained by different factors. First, the volume of $\text{Co}^{2+}\text{Fe}^{3+}\text{F}_5(\text{H}_2\text{O})_2$ was obtained by single crystal refinement comparing to the other volumes obtained by powder refinement with low quality

data. Second, it may have unit cell volume dilatation since the PXRD patterns were measured at 393 K (compared to 300 K for $\text{Co}^{2+}\text{Fe}^{3+}\text{F}_5(\text{H}_2\text{O})_2$ crystal).

The volume of $\text{M}^{2+}\text{Fe}_2\text{F}_8(\text{H}_2\text{O})_2$ is quite constant according the evolution of x_{exp} (between 366 and 367 \AA^3) and a bit superior to $\text{Co}^{2+}\text{Fe}_2\text{F}_8(\text{H}_2\text{O})_2$ extracted from Lemoine *et al.* work.¹ Here also, this difference could be explained by the dilatation of the unit cell volume. So, this trend suggests that only $\text{CoFe}_2\text{F}_8(\text{H}_2\text{O})_2$ is generated, without Fe^{2+} substitution.

To conclude, we have a full solid solution $(\text{Co}_{1-x}\text{Fe}_x)^{2+}\text{Fe}^{3+}\text{F}_5(\text{H}_2\text{O})_2$ and in parallel the formation of $\text{Co}^{2+}\text{Fe}_2\text{F}_8(\text{H}_2\text{O})_2$, and additionally for $x \geq 0.45$, the apparition of $\text{Fe}_2\text{F}_5(\text{H}_2\text{O})_2$ and $\text{Fe}_3\text{F}_8(\text{H}_2\text{O})_2$.

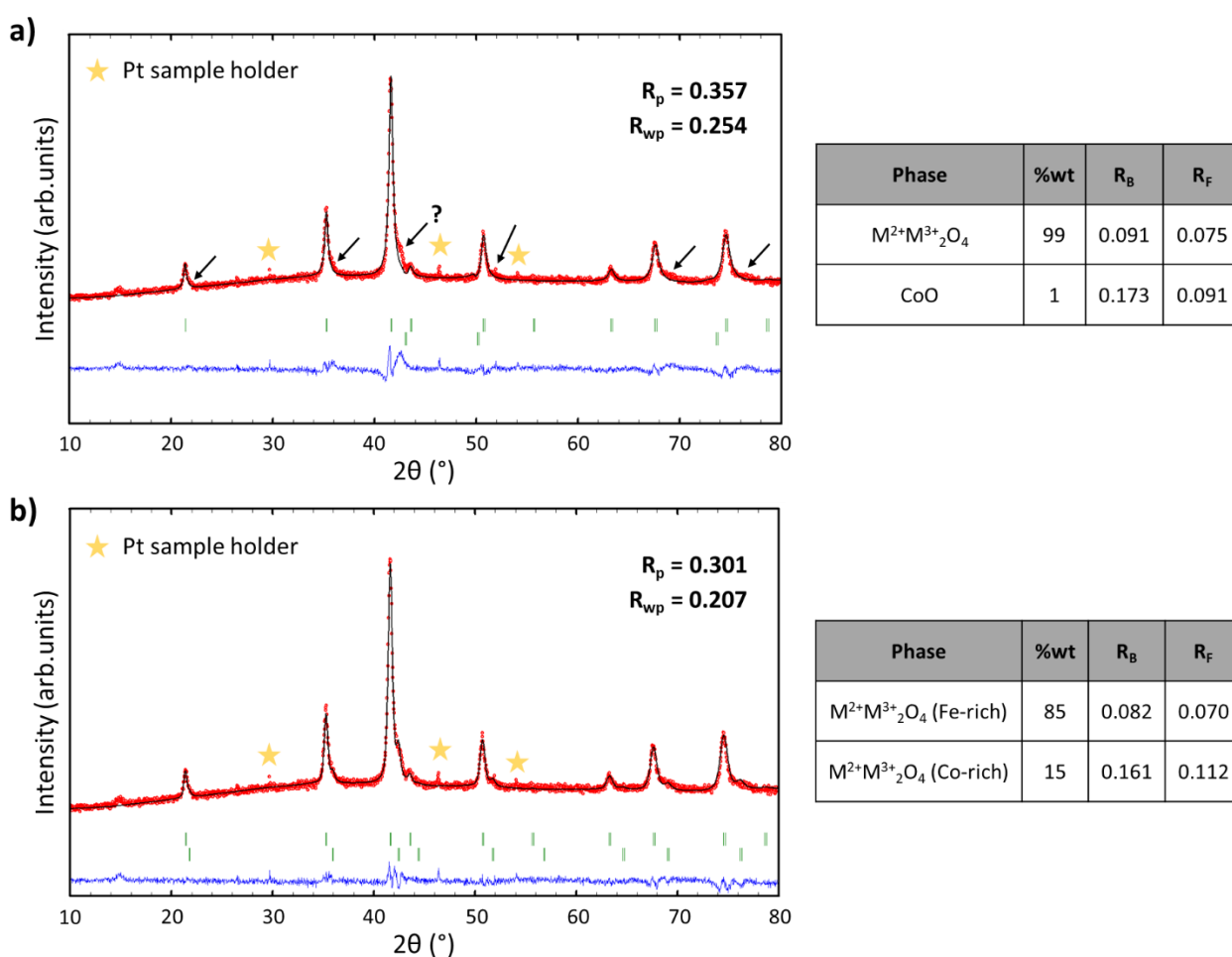


Figure S17: Rietveld refinements of the PXRD patterns of the $\text{Co}^{2+}\text{Fe}^{3+}\text{F}_5(\text{H}_2\text{O})_7$ ($x = 0$) at room temperature after thermal decomposition. The upper considers a spinel-type oxide $\text{M}^{2+}\text{M}^{3+}_2\text{O}_4$ ($\text{M} = \text{Co}$ and/or Fe) and CoO and the lower one considers two spinel-type oxides.

From the Rietveld refinement (lower one), we obtained the volumes of 583 \AA^3 for phase n°1 and 552 \AA^3 for phase n°2, respectively attributed to Fe-rich spinel $\text{Co}^{2+}(\text{Co}_{0.24}\text{Fe}_{1.76})^{3+}\text{O}_4$ and Co-rich spinel $\text{Co}^{2+}(\text{Co}_{1.17}\text{Fe}_{0.83})^{3+}\text{O}_4$, calculated according to **Figure S18**.

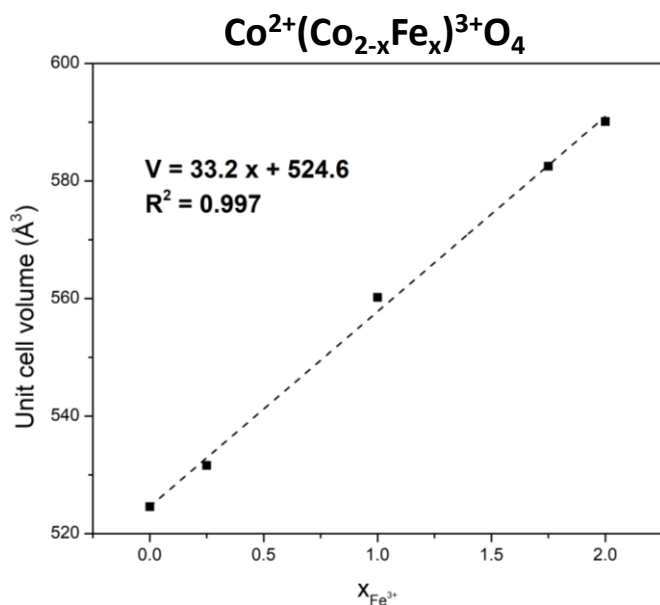


Figure S18: Evolution of the unit cell volume of different compositions extracted from the solid solution $Co^{2+}(Co_{2-x}Fe_x)^{3+}O_4$, taking from the literature.

Materials taken from the literature: Co_3O_4 (ICSD n°27498), $Co_{2.75}Fe_{0.25}O_4$ (ICSD n°12807), Co_2FeO_4 (ICSD n°98552), $Co_{1.25}Fe_{1.75}O_4$ (ICSD n°17714) and $CoFe_2O_4$ (ICSD n°33181).

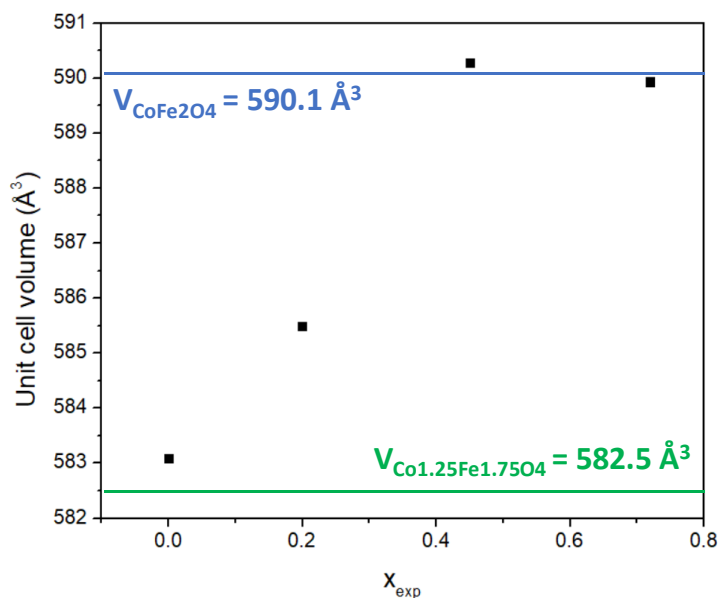


Figure S19: Volume refined of Fe-rich spinel obtained by Le Bail refinements of the different $(Co_{1-x}Fe_x)^{2+}Fe^{3+}F_5(H_2O)_7$ PXRD patterns measured at room temperature after thermal decomposition.

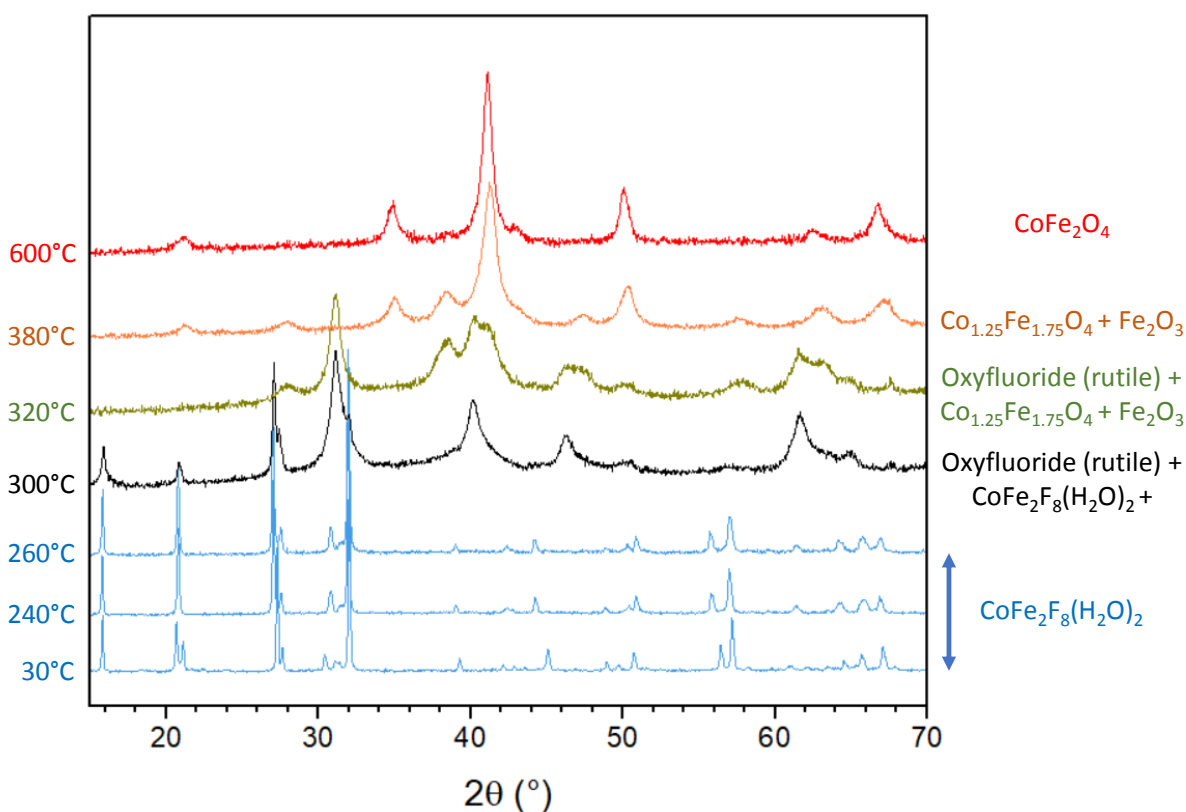


Figure S20: Thermal evolution of the X-ray diffractograms for $\text{Co}^{2+}\text{Fe}_2\text{F}_8(\text{H}_2\text{O})_2$ under ambient air.

The thermal degradation of $\text{Co}^{2+}\text{Fe}_2\text{F}_8(\text{H}_2\text{O})_2$ leads to a rutile oxyfluoride with same chemical composition as the one issued from $\text{Co}^{2+}\text{Fe}^{3+}\text{F}_5(\text{H}_2\text{O})_2$ according to **Figure S16**, e.g. $\text{Co}_{0.5}\text{Fe}_{0.5}\text{O}_{0.5}\text{F}_{1.5}$, and probably also some amorphous- FeF_3 which gives birth to Fe_2O_3 later. Oxyfluoride is decomposed further in $\text{Co}_{1.25}\text{Fe}_{1.75}\text{O}_4$ which seems to react with remaining Fe_2O_3 giving pure CoFe_2O_4 at high temperatures as attested by the shift towards small diffraction angles.

Table S13. Calcination conditions (temperature and time), weight loss of the hydrated precursors leading to the oxyfluorides and the corresponding specific surface area (S_{BET}).

Hydrated Fluorides	T_{calci} (°C)	t_{calci} (min)	Theo. weight loss (wt. %)	Exp. weight loss (wt. %)	Oxyfluorides (theoretical formulation)	S_{BET} ($\text{m}^2 \cdot \text{g}^{-1}$)
$\text{Co}^{2+}\text{Fe}^{3+}\text{F}_5(\text{H}_2\text{O})_7$	330	55	44.1	43.9	$\text{Co}_{0.5}\text{Fe}_{0.5}\text{O}_{0.5}\text{F}_{1.5}$	63
$(\text{Co}_{0.8}\text{Fe}_{0.2})^{2+}\text{Fe}^{3+}\text{F}_5(\text{H}_2\text{O})_7$	340	44	44.3	44.8	$\text{Co}_{0.4}\text{Fe}_{0.6}\text{O}_{0.6}\text{F}_{1.4}$	67
$(\text{Co}_{0.55}\text{Fe}_{0.45})^{2+}\text{Fe}^{3+}\text{F}_5(\text{H}_2\text{O})_7$	330	40	44.7	44.4	$\text{Co}_{0.275}\text{Fe}_{0.725}\text{O}_{0.725}\text{F}_{1.275}$	83
$(\text{Co}_{0.28}\text{Fe}_{0.72})^{2+}\text{Fe}^{3+}\text{F}_5(\text{H}_2\text{O})_7$	280	60	45.0	45.3	$\text{Co}_{0.14}\text{Fe}_{0.86}\text{O}_{0.86}\text{F}_{1.14}$	79

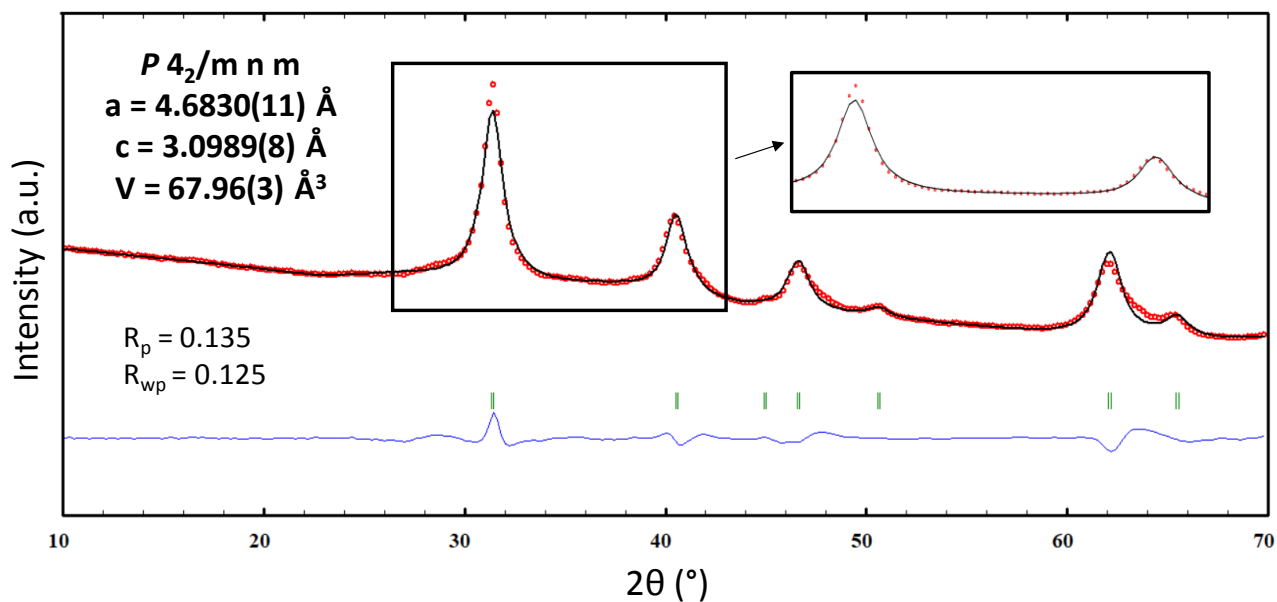


Figure S21: Le Bail refinement of calcined $\text{Co}^{2+}\text{Fe}^{3+}\text{F}_5(\text{H}_2\text{O})_7$.

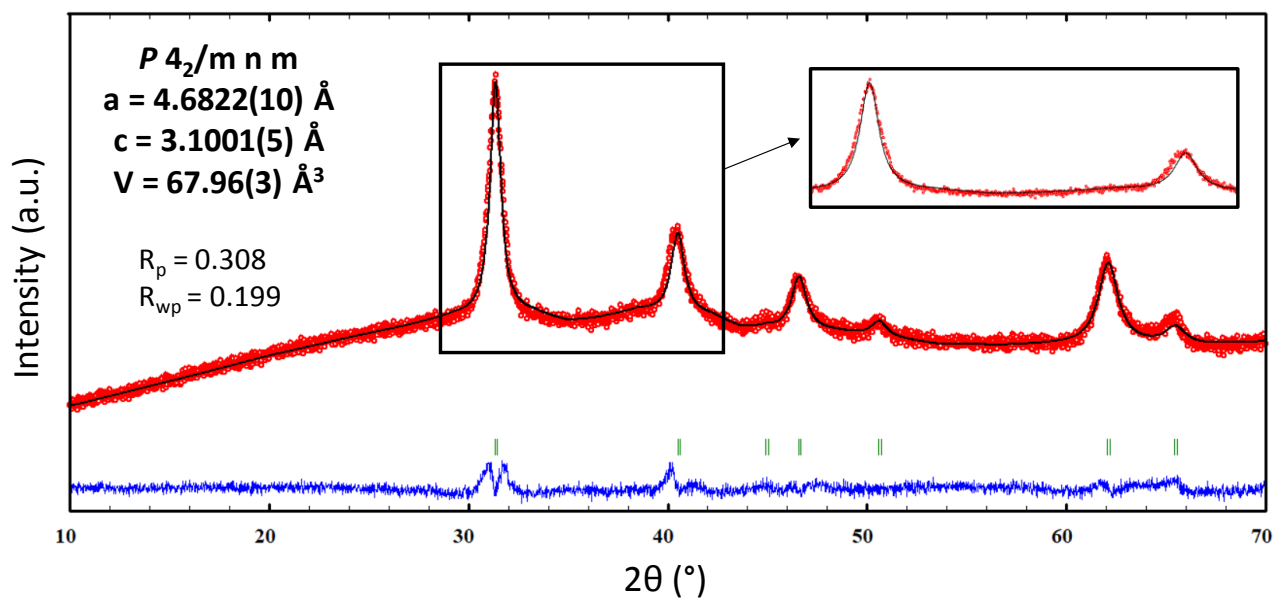


Figure S22: Le Bail refinement of calcined $(\text{Co}_{0.8}\text{Fe}_{0.2})^{2+}\text{Fe}^{3+}\text{F}_5(\text{H}_2\text{O})_7$.

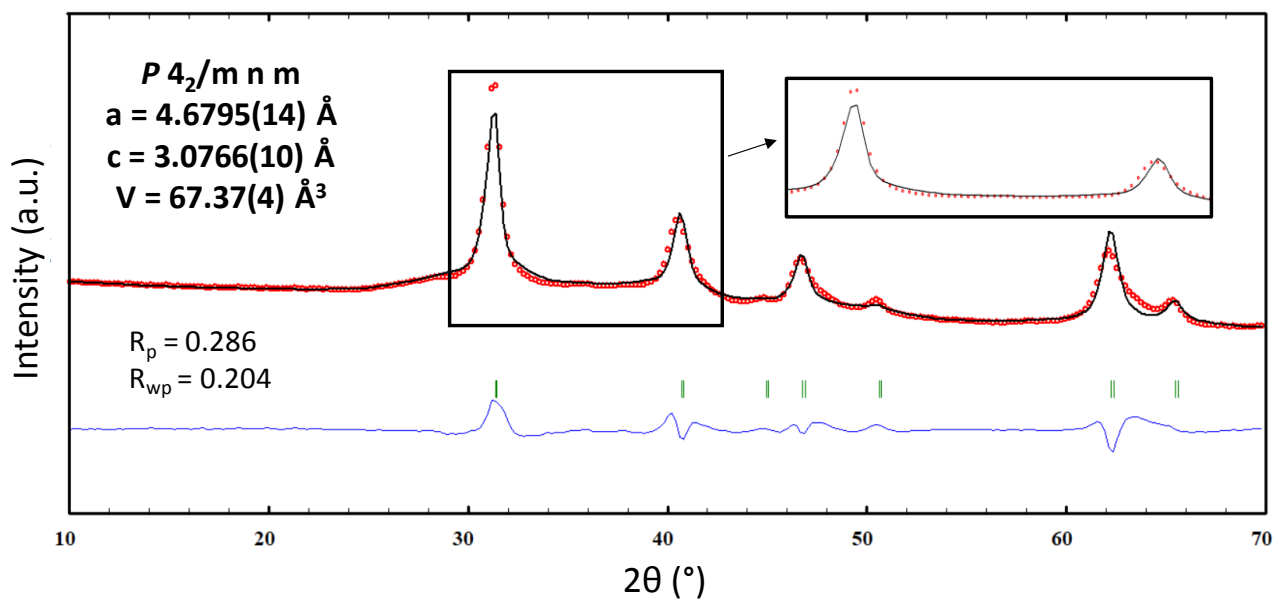


Figure S23: Le Bail refinement of calcined $(\text{Co}_{0.55}\text{Fe}_{0.45})^{2+}\text{Fe}^{3+}\text{F}_5(\text{H}_2\text{O})_7$.

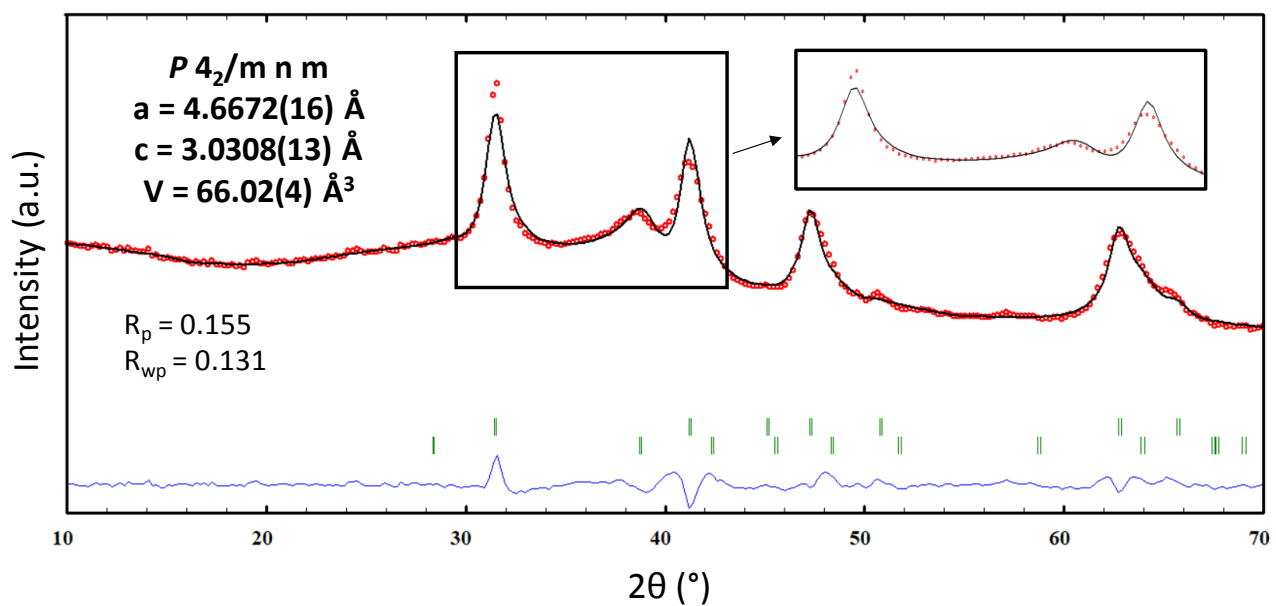


Figure S24: Le Bail refinement of calcined $(\text{Co}_{0.28}\text{Fe}_{0.72})^{2+}\text{Fe}^{3+}\text{F}_5(\text{H}_2\text{O})_7$.

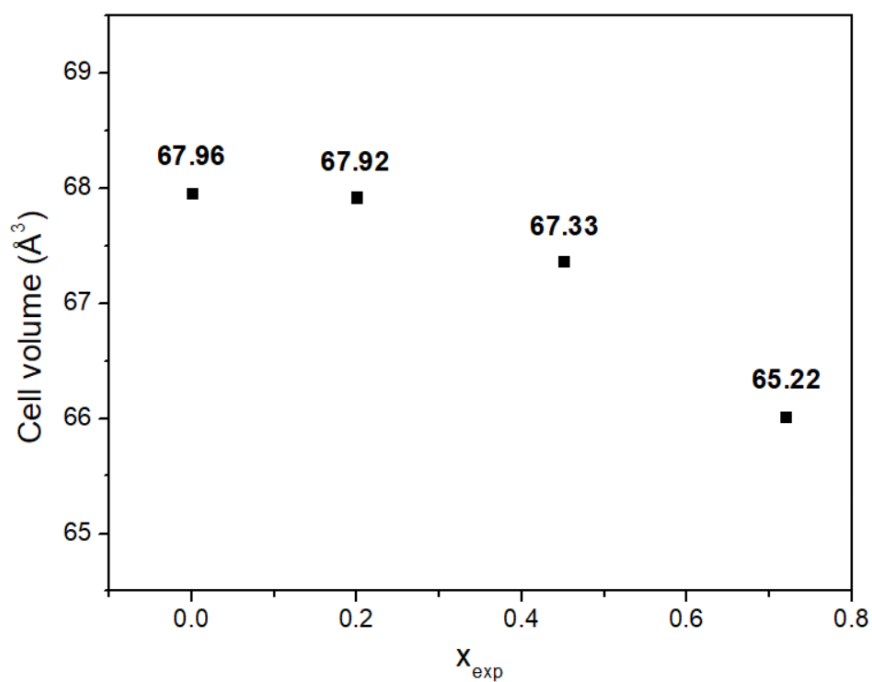


Figure S25: Evolution of the unit cell volume of the rutile oxyfluoride phase, extracted from Le Bail refinements.

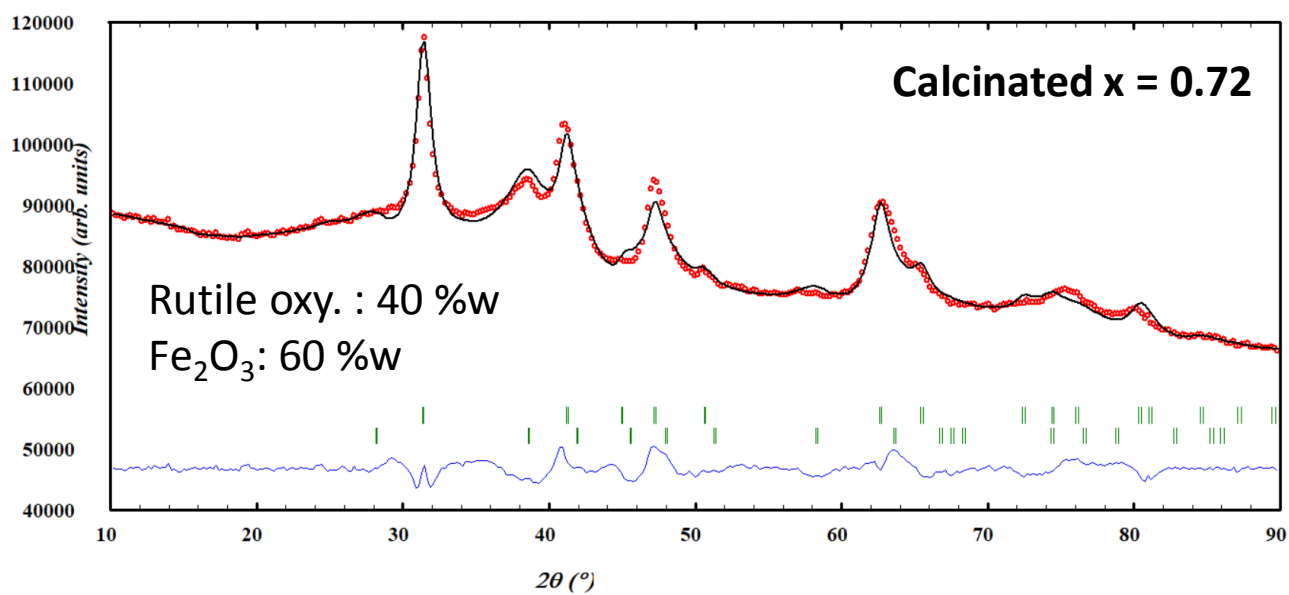
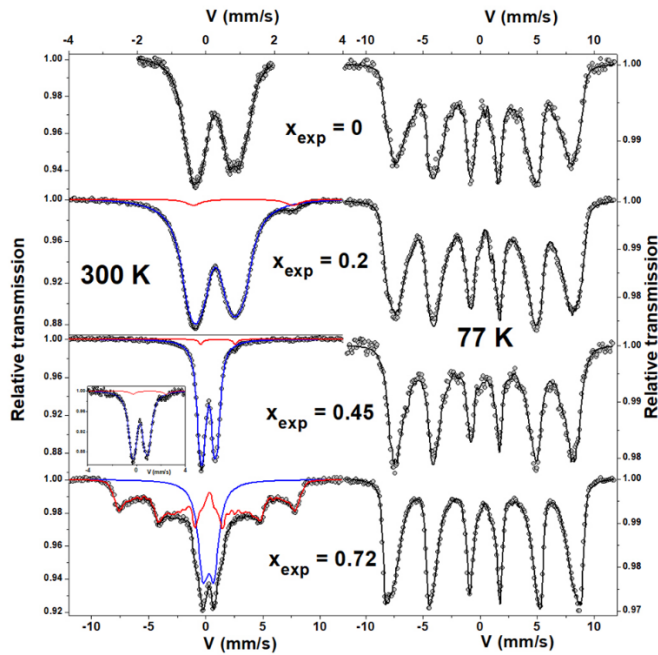
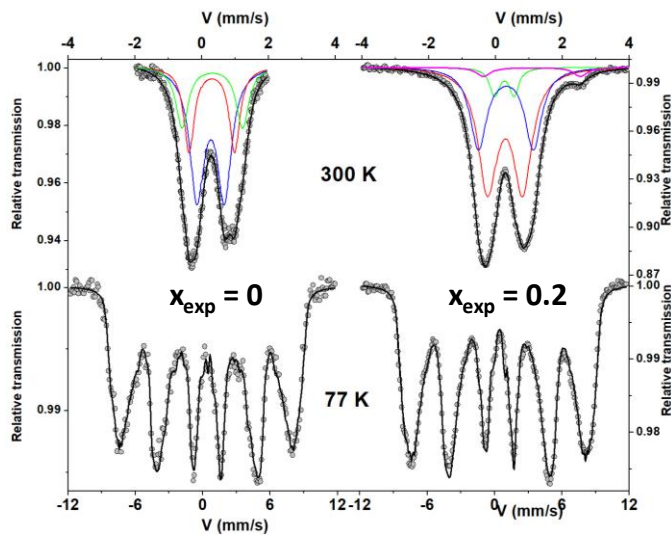


Figure S26: Rietveld refinement of the sample obtained after calcination of $(\text{Co}_{0.28}\text{Fe}_{0.72})^{2+}\text{Fe}^{3+}\text{F}_5(\text{H}_2\text{O})_7$.



	T (K)	Fe ⁿ⁺	IS (mm/s) ± 0.02	ΔE _Q /ρ2ε (mm/s) ± 0.02	B _{hf} (T) ± 0.5	% ± 2
x _{exp} = 0	300	Fe ³⁺	<0.41>	<1.16>	-	100
	77	Fe ³⁺	<0.52>	<-0.07>	<39.2>	100
x _{exp} = 0.20	300	Fe ³⁺ Fe ²⁺	<0.41> 1.21	<1.20> 2.87	- -	97 3
	77	Fe ³⁺	<0.53>	<-0.05>	<41.7>	100
x _{exp} = 0.45	300	Fe ³⁺ Fe ²⁺	<0.41> 1.20	<1.21> 2.69	- -	97 3
	77	Fe ³⁺	<0.53>	<-0.03>	<42.3>	100
x _{exp} = 0.72	300	Fe ³⁺ Fe ³⁺	0.23 0.188	0.88 <-0.13>	- <33.2>	33 67
	77	Fe ³⁺	<0.52>	<-0.12>	<44.1>	100

Figure S27: ⁵⁷Fe Mössbauer spectra and refined values of the hyperfine parameters resulting from the ⁵⁷Fe Mössbauer spectra of the calcined (Co_{1-x}Fe_x)²⁺Fe³⁺F₅(H₂O)₇ samples at 300 K and 77 K.



	T (K)	Fe ⁿ⁺	IS (mm/s) ± 0.02	ΔE _Q /ρ2ε (mm/s) ± 0.02	B _{hf} (T) ± 0.5	% ± 2
x _{exp} = 0	300	Fe ³⁺	0.39	0.81	-	54
		Fe ³⁺	0.43	1.35	-	23
		Fe ³⁺	0.44	1.79	-	23
	77	Fe ³⁺	<0.52>	<-0.07>	<39.2>	100
x _{exp} = 0.2	300	Fe ³⁺	0.38	0.57	-	6
		Fe ³⁺	0.40	1.02	-	57
		Fe ³⁺	0.43	1.61	-	34
		Fe ²⁺	1.21	2.87	-	3
	77	Fe ³⁺	<0.53>	<-0.05>	<41.7>	100

Figure S28: Comparison of ⁵⁷Fe Mössbauer spectra and refined values of the hyperfine parameters resulting from the ⁵⁷Fe Mössbauer spectra of the calcined Co²⁺Fe³⁺F₅(H₂O)₇ and (Co_{0.8}Fe_{0.2})²⁺Fe³⁺F₅(H₂O)₇ samples at 300 K and 77 K. Blue, red and green lines correspond to Fe³⁺ quadrupolar components while pink line refers to Fe²⁺ quadrupolar component.

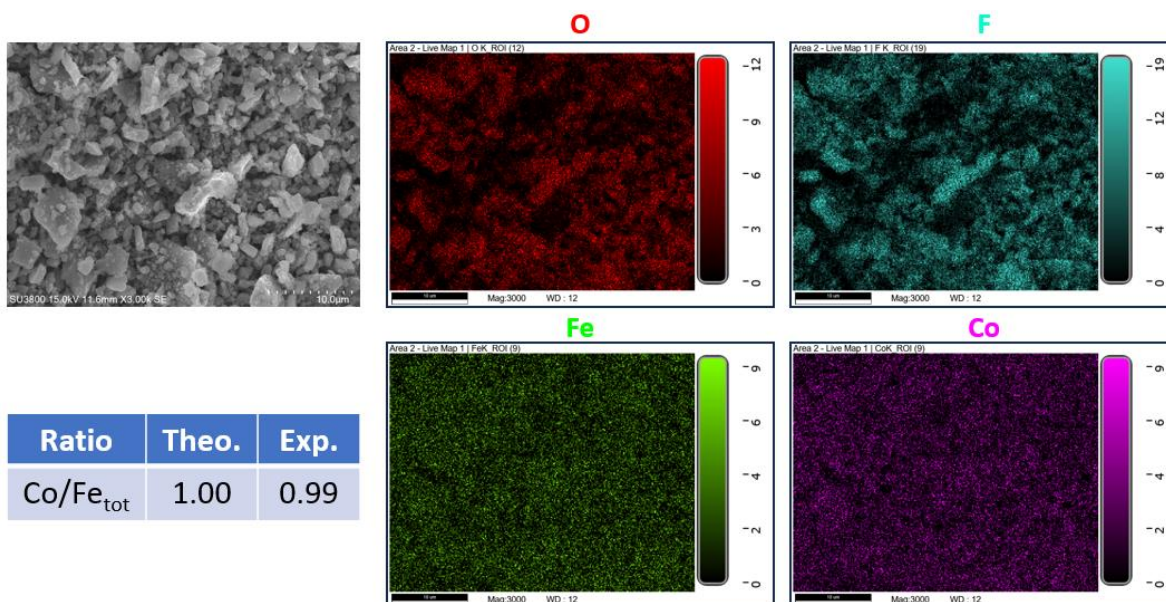


Figure S29: SEM images and elemental mapping of calcined $\text{Co}^{2+}\text{Fe}^{3+}\text{F}_5(\text{H}_2\text{O})_7$.

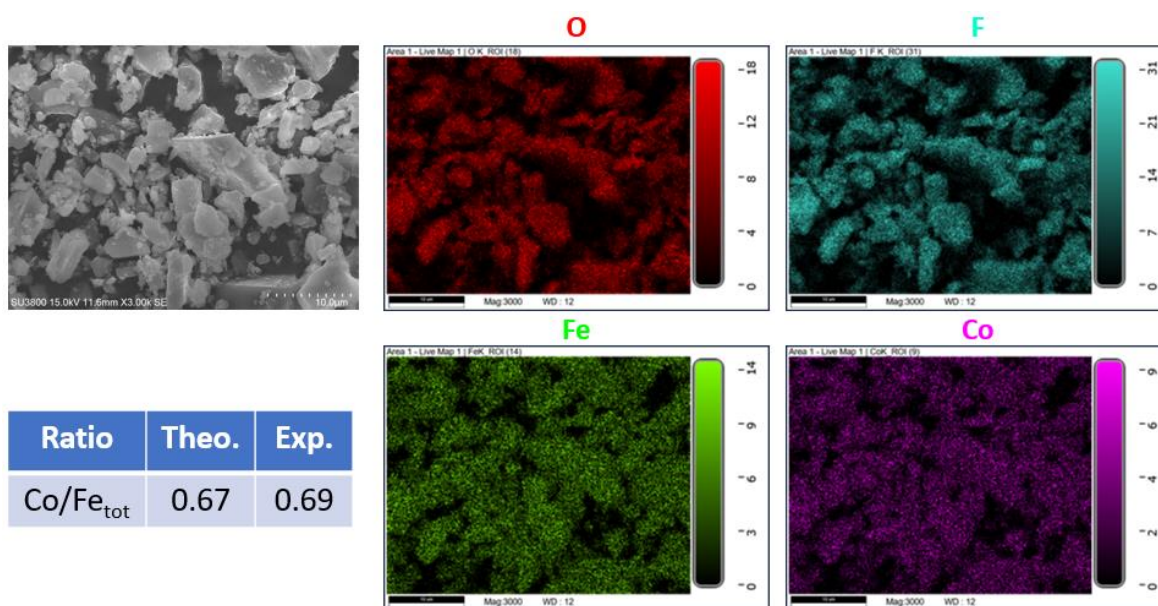


Figure S30: SEM images and elemental mapping of calcined $(\text{Co}_{0.8}\text{Fe}_{0.2})^{2+}\text{Fe}^{3+}\text{F}_5(\text{H}_2\text{O})_7$.

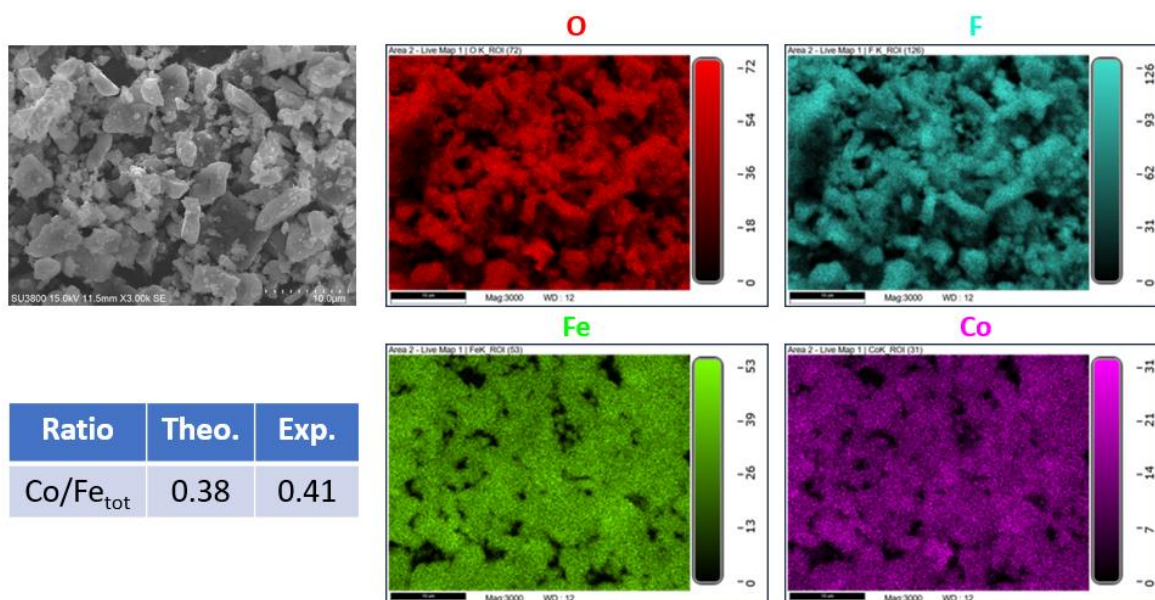


Figure S31: SEM images and elemental mapping of calcined $(\text{Co}_{0.55}\text{Fe}_{0.45})^{2+}\text{Fe}^{3+}\text{F}_5(\text{H}_2\text{O})_7$.

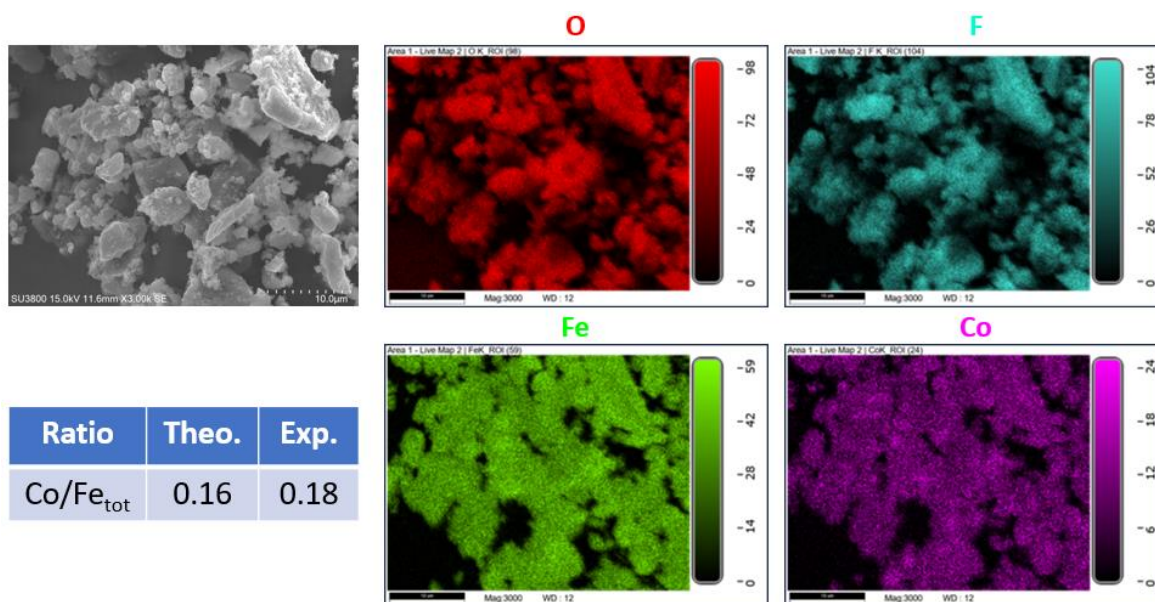


Figure S32: SEM images and elemental mapping of calcined $(\text{Co}_{0.28}\text{Fe}_{0.72})^{2+}\text{Fe}^{3+}\text{F}_5(\text{H}_2\text{O})_7$.

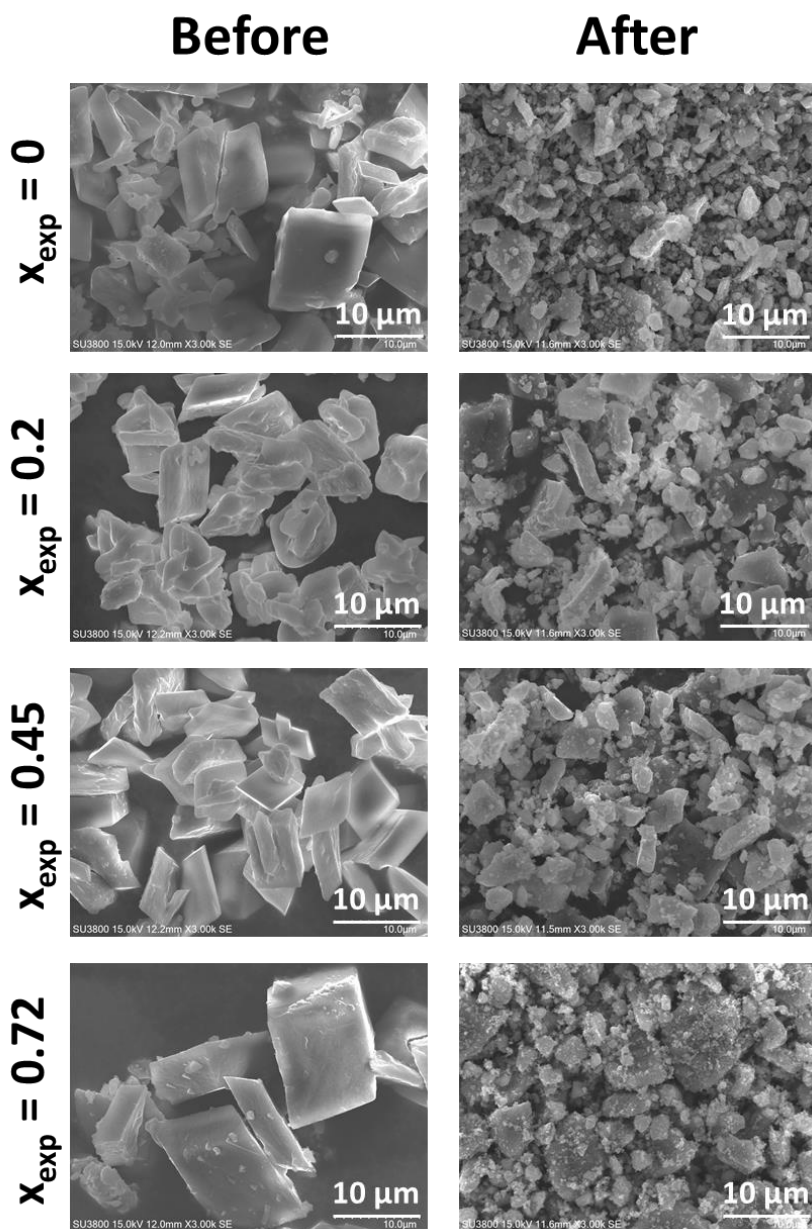


Figure S33: SEM images of $(\text{Co}_{1-x}\text{Fe}_x)^{2+}\text{Fe}^{3+}\text{F}_5(\text{H}_2\text{O})_7$ before and after calcination, leading to oxyfluorides.

Table S14. ICP-OES analysis of Co and Fe of calcined $(\text{Co}_{1-x}\text{Fe}_x)^{2+}\text{Fe}^{3+}\text{F}_5(\text{H}_2\text{O})_7$

	Theo./Exp. concentrations (ppm)		Theo./Exp. Metal %w in sample		Theo./Exp. molar ratio
	Fe	Co	Fe	Co	n(Co)/n(Fe)
$x_{\text{exp}} = 0$	10.1/9.84	10.61/10.82	29.7/29.1	31.4/32.0	1/1.04
$x_{\text{exp}} = 0.2$	3.66/3.66	2.58/2.57	35.9/35.9	25.3/25.2	0.67/0.66
$x_{\text{exp}} = 0.45$	4.46/3.89	1.79/1.38	43.8/38.1	17.5/13.5	0.38/0.34
$x_{\text{exp}} = 0.72$	5.13/4.53	0.88/0.70	52.4/46.2	9.0/7.2	0.16/0.15

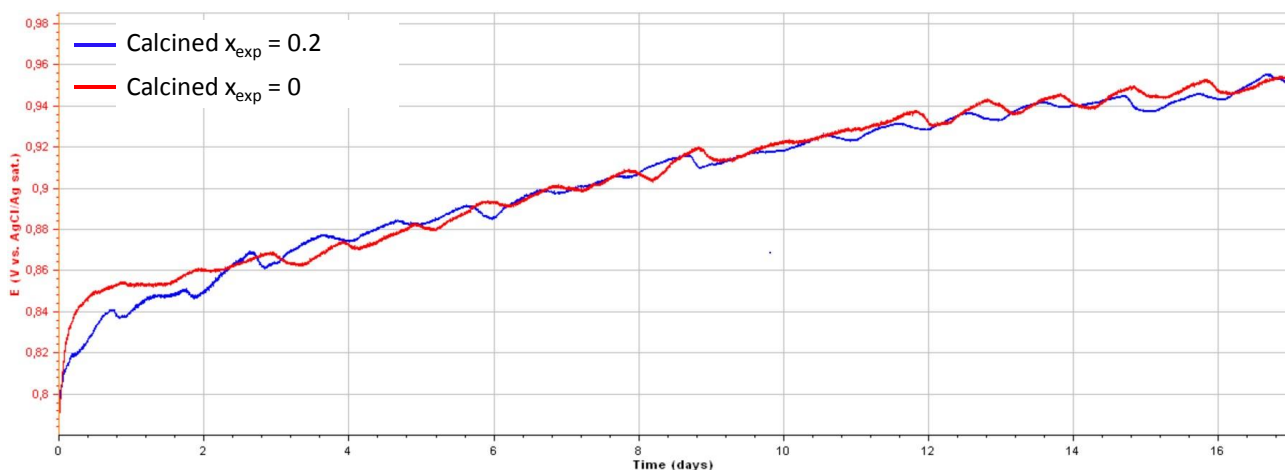


Figure S34: Chronopotentiometric measurement at $125 \text{ mA}\cdot\text{cm}^{-2}$ in 1M KOH of calcined $x_{\text{exp}} = 0$ and 0.2 .

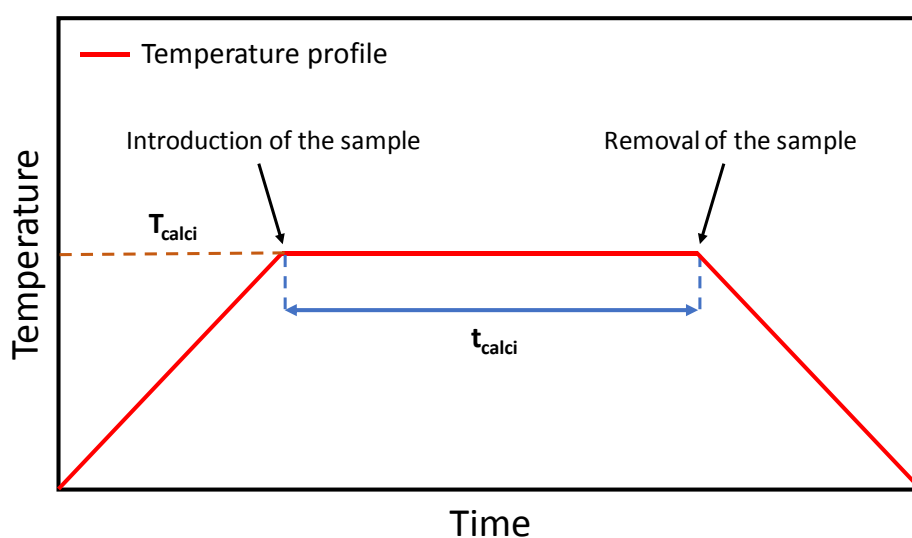


Figure S35: Temperature profile of the muffle furnace to prepare the calcined $(\text{Co}_{1-x}\text{Fe}_x)^{2+}\text{Fe}^{3+}\text{F}_5(\text{H}_2\text{O})_7$.

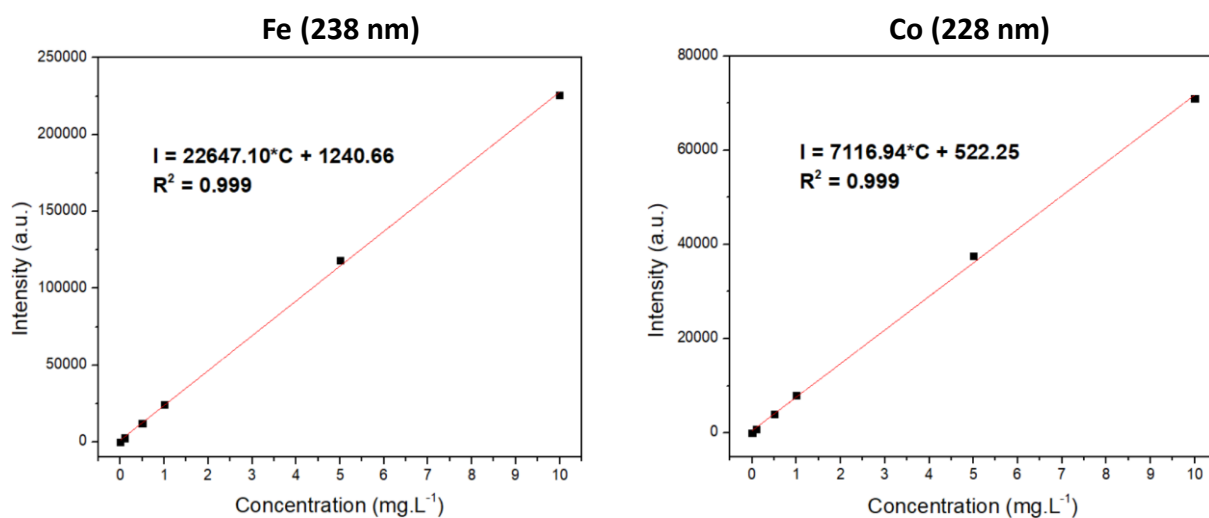


Figure S36: ICP-OES calibration curves for the element Fe (238 nm) and Co (228 nm).

References

- (1) Lemoine, K.; Zhang, L.; Grenèche, J. M.; Hémon-Ribaud, A.; Leblanc, M.; Guet, A.; Galven, C.; Tarascon, J. M.; Maisonneuve, V.; Lhoste, J. New Amorphous Iron-Based Oxyfluorides as Cathode Materials for High-Capacity Lithium-Ion Batteries. *J. Phys. Chem. C* **2019**, *123* (35), 21386–21394. <https://doi.org/10.1021/acs.jpcc.9b06055>.